Breaking of vortex lines as a forerunner of the developed Kolmogorov turbulence

E.A. Kuznetsov

Lebedev Physical Institute, Moscow, Russia

Landau Institute for Theoretical Physics, Moscow, Russia

Novosibirsk State University, Novosibirsk, Russia

Joined with:

D.S. Agafontsev (Shirshov Institute & NSU),

A.A. Mailybaev (MSU Institute of Mechanics & IMPA, Brazil)

A.N. Kudryavtsev (Khristianovich ITAM, Novosibirsk)

E.V. Sereshchenko (NSU & Khristianovich ITAM, Novosibirsk)

OUTLINE

- Motivation: Collapses and Kolmogorov spectrum

- Vortex line representation and new Cauchy invariant

- Folding of vortex lines

- Self-similar asymptotics

- Numerical experiment

- Tendency to breaking in 2D turbulence

- Numerical experiments for 2D decay turbulence

- 2D turbulence with pumping and viscous-type damping

Collapses and Kolmogorov spectrum

- (1941) <u>Kolmogorov-Obukhov spectrum</u>, i.e. the energy distribution of the velocity fluctuations in the inertial interval ($Re \gg 1$), $E_k \sim P^{2/3}k^{-5/3}$ where P is the energy flux. This spectrum can be obtained from the dimensional analysis.

  E_k has the meaning of the energy density in the phase space ϵ_k, multiplied by $4\pi k^2$. Thus, according to the dimensional analysis

  $$\epsilon_k = \frac{\rho c^2}{k^3} F\left(\frac{P}{\rho c^2 kc}\right).$$

  Of course, light speed c can not stand here. Hence we immediately get the Kolmogorov answer.

Collapses and Kolmogorov spectrum

- The Kolmogorov theory is based on two very important assumptions:
  1. Turbulence in the inertial interval is assumed isotropic and homogeneous.
  2. Nonlinear interaction in this interval is supposed local and defined by P only.

- It is well known that singularities give the power type behavior of the Fourier amplitudes that provides appearance of power tails for turbulent spectra.

Collapses and Kolmogorov spectrum

- Using the dimensional analysis one can get that the energy transfer time T from large scales L to dissipative ones is finite and defined by L and P : $T \sim L^{2/3}P^{-1/3}$.

- Distribution of velocity fluctuations
$$< \delta v > \sim P^{1/3}r^{1/3}$$
Respectively, for fluctuations of vorticity $\omega = [\nabla \times \mathbf{v}]$ we have:
$$\delta\omega \sim P^{1/3}r^{-2/3}.$$

  Thus, for ω we have singularity at $r \to 0$, besides T is finite.

- <u>Questions:</u> Is it a real singularity? Is it possible to say that the Kolmogorov spectrum appears as a result of collapse, i.e. the formation of singularity in a finite time?

Collapses and Kolmogorov spectrum

In this lecture, based on both the vortex line representation (VLR) and direct numerical integration of 3D Euler, we show that:

- At the stage of turbulence arising the spectrum is very far from isotropic (in the inertial interval).

- The main contribution in the spectrum in 3D is connected with appearance of coherent structures of the pancake type which in the turbulent spectrum are responsible for jets with growing in time anisotropy. (First time such structures were observed in numerical experiments by M. Brachet, et. el. (1992).)

- The maximal pancake vorticity and its width ℓ are connected by means of the Kolmogorov type relation:

$$\omega_{max} \sim \ell^{-2/3}.$$

Collapses and Kolmogorov spectrum

- Appearance of the pancake structures is a consequence of folding (breaking) of the vorticity lines which develops in time exponentially. Possibility of folding (breaking) is connected with compressibility of vortex lines as it follows from the vortex line representation (K. & Ruban, 1998, K. 2002).

- Increasing with time number of such structures leads to formation of the Kolmogorov energy spectrum observed numerically in a fully inviscid flow, with no tendency towards finite-time blowup.

Collapse of the vorticity - naive arguments

At $Re \gg 1$ in the inertial range one can use the Euler equation which for ω reads as

$$\frac{d\omega}{dt} = (\omega \cdot \nabla)\mathbf{v}, \ \ \frac{d}{dt} = \frac{\partial}{\partial t} + (\mathbf{v} \cdot \nabla), \ \ \text{div } \mathbf{v} = 0.$$

At the maximal point ω_{max} satisfies the equation

$$\frac{d\omega_{max}}{dt} = \frac{\partial v_\tau}{\partial x_\tau} \, \omega_{max}.$$

where $\tau = \omega/|\omega|$. If $\frac{\partial v_\tau}{\partial x_\tau} = \alpha\omega_{max}$ then we have the ODE, $d\omega_{max}/dt = \alpha\, \omega_{max}^2$, with the blow-up solution:

$$\omega_{max} \sim (t_0 - t)^{-1}.$$

VLR and new Cauchy invariant

It is well known that the Euler equation

$$\frac{\partial \mathbf{v}}{\partial t} + (\mathbf{v}\nabla)\mathbf{v} = -\nabla p, \qquad \text{div } \mathbf{v} = 0,$$

has infinite (continuous) number of integrals of motion. These are the so called Cauchy invariants. They can be obtained from the Kelvin theorem

$$\Gamma = \oint_{C[t]} (\mathbf{v} \cdot d\mathbf{l}) = \text{inv}$$

with the movable together with fluid contour $C[t]$. Passing in this integral to the Lagrangian variables,

$$\mathbf{r} = \mathbf{r}(\mathbf{a}, t), \ \ \frac{d\mathbf{r}}{dt} = \mathbf{v}(\mathbf{r}, t), \ \ \mathbf{r}|_{t=0} = \mathbf{a}$$

we arrive at

$$\Gamma = \oint_{C[a]} \dot{x}_i \cdot \frac{\partial x_i}{\partial a_k} \, da_k \ , \ \text{ with fixed } C[a].$$

VLR and new Cauchy invariant

Hence we get the Cauchy invariants

$$\mathbf{I} = \mathsf{rot}_a \left(\dot{x}_i \frac{\partial x_i}{\partial \mathbf{a}} \right) \equiv \omega_{\mathbf{0}}(\mathbf{a})$$

which are constraints in Euler. They characterize the frozenness of the vorticity into fluid. The latter means that fluid (Lagrangian) particles can not leave its own vortex line where they were initially. Thus, the particles have one independent degree of freedom – motion along vortex line. But such a motion does not change the vorticity:

$$\frac{\partial \omega}{\partial t} = \mathsf{rot} \, [\mathbf{v} \times \omega].$$

VLR and new Cauchy invariant

Thus, the Helmholtz equation contains only one velocity component normal to the vortex line, $\mathbf{v_n}$. The tangent velocity $\mathbf{v_\tau}$ plays a passive role providing incompressibility. Decomposing, $\mathbf{v} = \mathbf{v_n} + \mathbf{v_\tau}$, in the Euler *incompressible* equations leads to the equation of motion of charged *compressible* fluid moving in an electromagnetic field:

$$\frac{\partial \mathbf{v}_n}{\partial t} + (\mathbf{v}_n \nabla)\mathbf{v}_n = \mathbf{E} + [\mathbf{v}_n \times \mathbf{H}],$$

 where

$$\mathbf{E} = -\nabla \varphi - \frac{\partial \mathbf{A}}{\partial t}, \ \ \mathbf{H} = \text{rot } \mathbf{A}$$

with $\varphi = p + v_\tau^2/2, \ \mathbf{A} = \mathbf{v}_\tau$. Thus, two Maxwell equations are satisfied with the gauge: $\text{div } \mathbf{A} = -\text{div } \mathbf{v}_n \neq 0$.

VLR and new Cauchy invariant

Now perform transform in a new charged *compressible* hydrodynamics to the Lagrangian description:

$$\dot{\mathbf{r}} = \mathbf{v}_n(\mathbf{r}, t) \text{ with } \mathbf{r}|_{t=0} = \mathbf{a}.$$

Under this transform the new hydrodynamics become the Hamilton equations:

$$\dot{\mathbf{P}} = -\partial h/\partial \mathbf{r}, \qquad \dot{\mathbf{r}} = \partial h/\partial \mathbf{P},$$

$\mathbf{P} = \mathbf{v}_n + \mathbf{A} \equiv \mathbf{v}$ is the generalized momentum, and the Hamiltonian $h = (\mathbf{P} - \mathbf{A})^2/2 + \varphi \equiv p + \mathbf{v}^2/2$ ($\equiv$ the Bernoulli "invariant").

The Kelvin (Liouville) theorem says that $\Gamma = \oint (\mathbf{P} \cdot d\mathbf{R}) = \mathrm{inv}$.
Transform in Γ to new Lagrangian coordinates leads to a new Cauchy invariant :

$$\mathbf{I} = \mathrm{rot}_a \left(P_i \frac{\partial x_i}{\partial \mathbf{a}} \right) \equiv \omega_0(\mathbf{a}).$$

VLR and a new Cauchy invariant

Hence, one can see that the only one velocity component normal to the vortex line, $\mathbf{v_n}$, can change ω. To define ω it is enough to know all trajectories of the equation

$$\dot{\mathbf{r}} = \mathbf{v}_n(\mathbf{r}, t), \; \mathbf{r}|_{t=0} = \mathbf{a}$$

or, by another words, mapping $\mathbf{r} = \mathbf{r}(\mathbf{a}, t)$. In terms of this mapping the Helmholtz Eq. can be integrated:

$$\omega(\mathbf{r}, t) = \frac{(\omega_0(\mathbf{a}) \cdot \nabla_a)\mathbf{r}(\mathbf{a}, t)}{J(\mathbf{a}, t)}$$

where $J(\mathbf{a}, t) = \partial(\mathbf{r})/\partial(\mathbf{a})$ is the Jacobian of the mapping. In this Eq. $\omega_0(\mathbf{a})$ is a new Cauchy invariant. Due to the vorticity frozenness, $\mathbf{v_n}$ is the velocity of vortex lines.

VLR and a new Cauchy invariant

These equations together with

$$\omega(\mathbf{r}, t) = \nabla_r \times \mathbf{v}(\mathbf{r}, t) \text{ and } \mathrm{div}_r \, \mathbf{v}(\mathbf{r}, t) = 0$$

form the complete system of equations in the vortex line representation (Kuznetsov, Ruban (1998), Kuznetsov (2002, 2006)).

In the general case, $\mathrm{div}_r \mathbf{v}_n \neq 0$ and therefore $\mathbf{r} = \mathbf{r}(\mathbf{a}, t)$ is the compressible mapping: the Jacobian is not fixed and can take arbitrary values! This means that continuously distributed vortex lines can be compressed.

The quantity $n = J^{-1}$ plays the role of vortex line density:

$$n_t + \mathrm{div}_r(n\mathbf{v}_n) = 0, \ \ \mathrm{div}_r \mathbf{v}_n \neq 0.$$

Folding of vortex lines

REMARK 1: Blowup, as wave breaking, is well known for compressible flows resulting in appearance of shocks, which can be considered as the formation of folds. Breaking in gasdynamics is possible due to compressible character of the mapping.

REMARK 2: Breaking/folding of vortex lines is impossible in 2D and for cylindrically symmetric flows without swirl (Majda, 1990) because $\omega \perp \mathbf{v}$ and $\mathrm{div}\,\mathbf{v}_n = 0$, and consequently $J = 1$.

Thus, breaking/folding of vortex lines is 3D phenomenon. Up to now it has not been known whether this process happens in a finite or infinite time.

Folding of vortex lines

In numerics, presented further, one can see, instead of blow-up, exponential increasing of the vorticity maximum and formation around this maximum a structure of the pancake type with exponential decreasing of its width. Such structures appear around each vorticity maximum. The process of pancake structure formation is shown to have self-similar behavior. (First time such structures were observed by M. Brachet, et. el. (1992).)

Geometrically it results in touching of vortex lines (it does not matter if this process happens in a finite or infinite time).
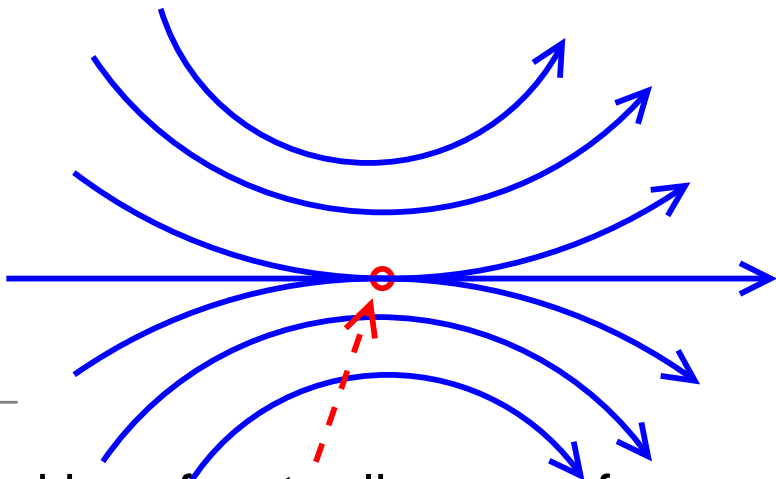
Folding of vortex lines

Let us assume that breaking/folding takes place. Consider the equation $J(\mathbf{a}, t) = 0$ and find its positive roots $t = \tilde{t}(\mathbf{a}) > 0$. Then the collapse (or touching) time will be

$$t_0 = \min_a \tilde{t}(\mathbf{a}).$$

Near the minimal point $\mathbf{a} = \mathbf{a}_0$ as the expansion of J takes the form:
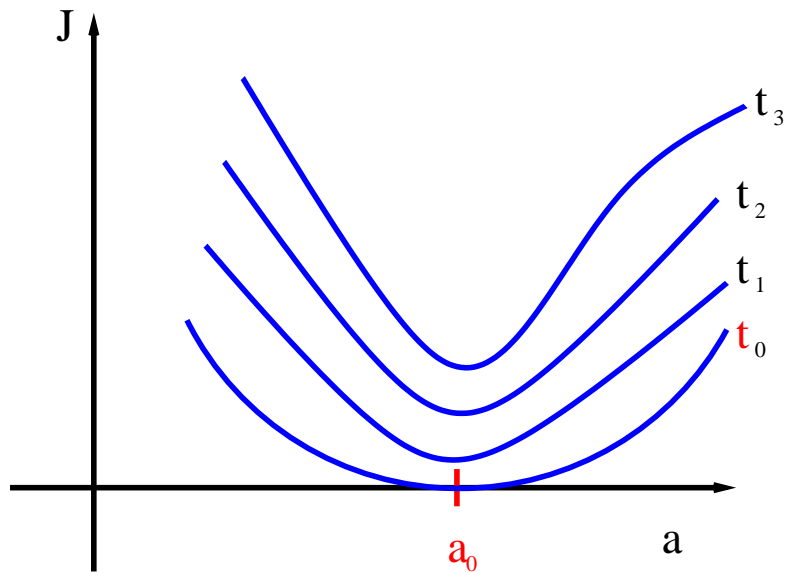
$$J(a, t) = \alpha \tau(t) + \gamma_{ij} \Delta a_i \Delta a_j$$

- concavity condition

$\alpha > 0$, $\tau(t) \to 0$ as $t \to t_0$,

γ_{ij} is positive definite (non-degenerate) time independent matrix,

$$\Delta \mathbf{a} = \mathbf{a} - \mathbf{a}_0.$$

$t_0 > t_1 > t_2 > t_3$

Self-similar asymptotics

REMARK: The assumption about linear dependence of J_{min} on $\tau(t)$ is familiar to the Landau assumption in his theory of the second-order phase transitions.

This expansion results in the self-similar asymptotics for vorticity:

$$\omega(\mathbf{r}, t) = \frac{(\omega_0(\mathbf{a}) \cdot \nabla_a)\mathbf{r}|_{a_0}}{\tau(\alpha + \gamma_{ij}\eta_i\eta_j)}, \quad \eta = \frac{\Delta a}{\tau^{1/2}}.$$

Now the main problem is
to transform from the auxiliary a-space to the physical $\mathbf{r}$-space.

Self-similar asymptotics

Consider first the 1D case when

$$J = \frac{\partial x}{\partial a} = \alpha\tau + \gamma a^2 \quad \rightarrow x = \alpha\tau a + \frac{1}{3}\gamma a^3.$$

Thus, $a \sim \tau^{1/2}, \ x \sim \tau^{3/2}$, i.e. in the physical space compression happens more rapidly than in the space of Lagrangian markers !! At distances $\gamma a^2 \gg \alpha\tau$ we have the time-independent asymptotics,

$$J \sim x^{2/3}.$$

Thus, any changes happen at the region $\gamma a^2 \leq \alpha\tau$.

Self-similar asymptotics

3D case

The Jacobian $J = \lambda_1 \lambda_2 \lambda_3 \to 0$ means that one eigenvalue,
say, $\lambda_1 \to 0$ and $\lambda_2, \lambda_3 \to$ const as $t \to t_0$ and $a \to a_0$. Hence it
follows that near singular point there are two different self
similarities:

along "soft" (λ_1) direction $x_1 \sim \tau^{3/2}$ (like in 1D);

along "hard" (λ_2, λ_3) directions $x_{2,3} \sim \tau^{1/2}$,

so that

$$\omega = \frac{1}{\tau} \mathbf{g} \left(\frac{x_1}{\tau^{3/2}}, \frac{x_\perp}{\tau^{1/2}} \right).$$
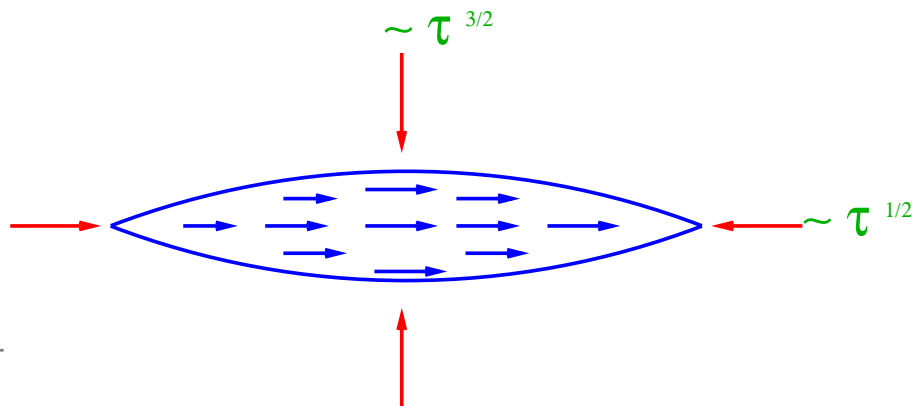
This results in formation

of pancake structure

(compare with Zeldovich)

Self-similar asymptotics

As $\tau \to 0$ when $\gamma_{ij}\Delta a_i \Delta a_j \gg \alpha\tau$ the vorticity has a time-independent, very anisotropic distribution. The main dependence of ω is connected with x_1-direction:

$$\omega \approx \frac{\mathbf{b}}{x_1^{2/3}}$$

with $\mathbf{b} = \text{const}$ and KOLMOGOROV index $2/3$!. This dependence is realized everywhere except regions between two cubic paraboloids $-cx_\perp^3 < x_1 < cx_\perp^3$ In this narrow region vorticity at $\tau = 0$ behaves like

$$\omega \approx \frac{\mathbf{b_1}}{x_\perp^2}.$$

Self-similar asymptotics
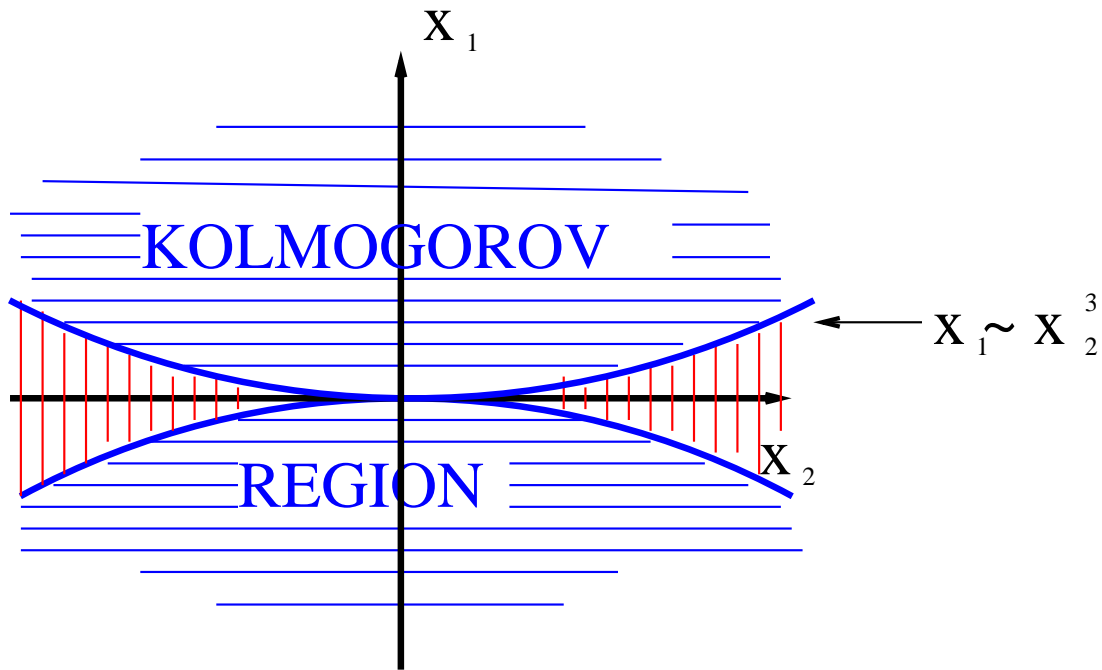
In Kolmogorov region the vorticity can be estimated as

$$\omega \sim \frac{P^{1/3}}{x_1^{2/3}}$$

where $P \sim \omega_0^3 L^2, \ L \sim \gamma^{-1/2}$.

Self-similar asymptotics

In the maximal point $\mathbf{a} = \mathbf{a_0}$ vorticity ω evidently grows like

$$\omega(t) \sim \tau^{-1} \sim \ell(t)^{-2/3}$$

where $\ell(t)$ is the pancake thickness.

At $\mathbf{a} = \mathbf{a_0}$ the enumerator in VLR can be written as

$$\hat{J}\omega_{\mathbf{0}} \approx \left(\lambda_2 \hat{P}_2 + \lambda_3 \hat{P}_3 \right) \omega_{\mathbf{0}} \perp \hat{P}_1 \omega_{\mathbf{0}}$$

where $\hat{P}_i$ is projector corresponding to λ_i. This means that the maximal vorticity lies in the plane perpendicular to the soft direction.

Numerical experiment

We use two numerical schemes based on direct integration of the Euler equations for ω and in the VLR formulation in the periodic box $\mathbf{r} = (x, y, z) \in [-\pi, \pi]^3$ using the pseudo-spectral method with high-order Fourier filtering. During simulations, the number of nodes is adapted independently along each coordinate providing an optimal anisotropic rectangular grid. We tested several large-scale initial conditions in the form of random truncated (up to second harmonics) Fourier series considered as a perturbation of the shear flow $\omega_x = \sin z, \ \omega_y = \cos z, \ \omega_z = 0$. This paper is based on one selected simulation with the final grid $486 \times 1024 \times 2048$.

Numerical experiment

- Formation of the pancake structures. The maximal pancake vorticity and its width ℓ are connected by means of the Kolmogorov type relation: $\omega_{max} \sim \ell^{-2/3}$.

- Fitting showed exponential increasing of the maximal vorticity and respectively exponential decreasing of the pancake width.

- By means of the VLR scheme it was demonstrated decreasing of the Jacobian. This means that formation of the pancake structures can be considered as folding (breaking) of the vorticity lines.

- Increasing with time number of such structures leads to formation of the Kolmogorov energy spectrum observed numerically in a fully inviscid flow.

Vorticity iso-surface (0.8 from ω_{max}), $t = 6.89$

(c)
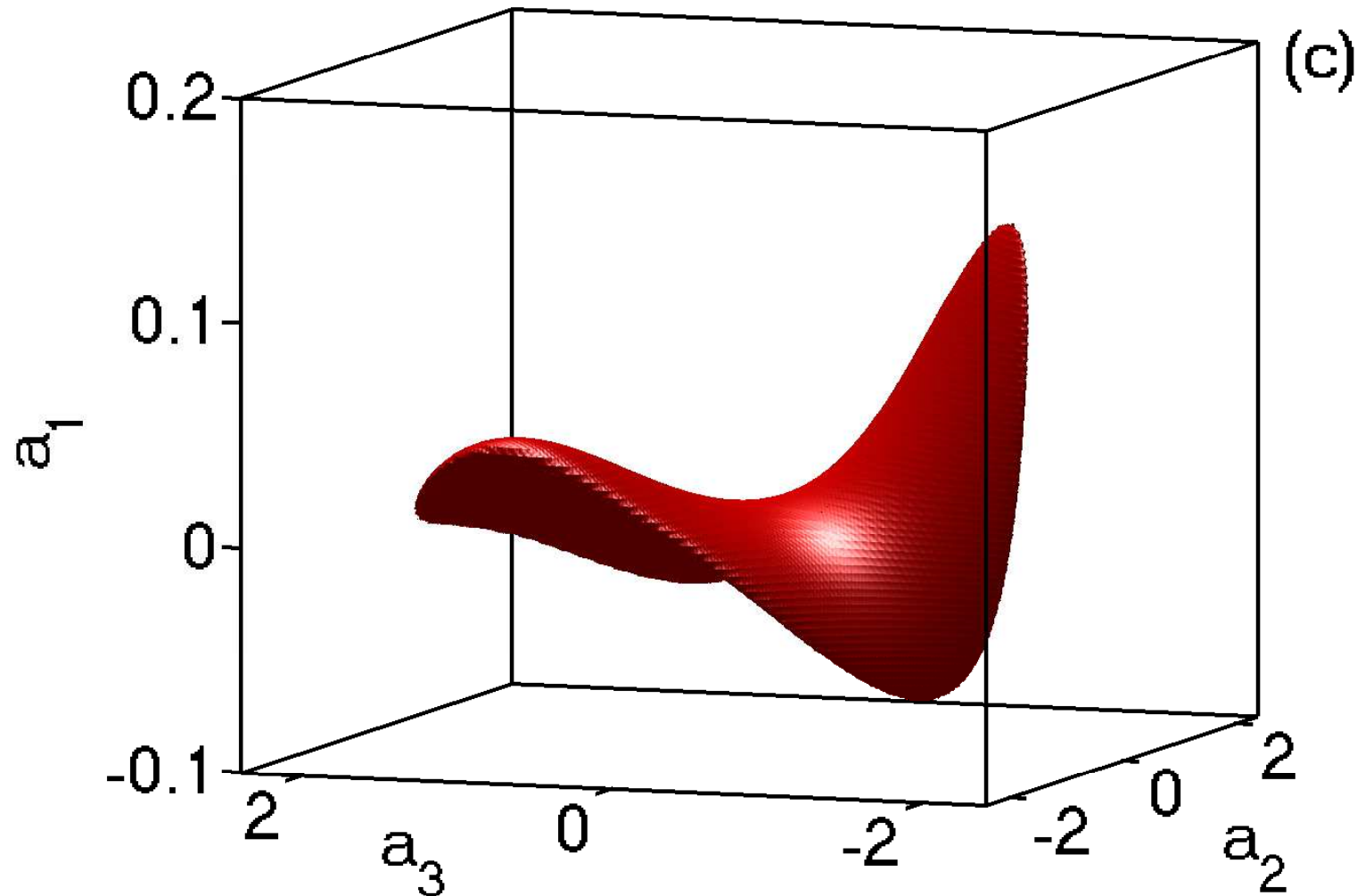
Numerical experiment: direct code, 2nd IC

Isosurface of vorticity $|\omega| = 0.8\,\omega_{\mathrm{max}}$ in local coordinates (χ_1, χ_2, χ_3) at the final time $t = 7.77$.

(a)
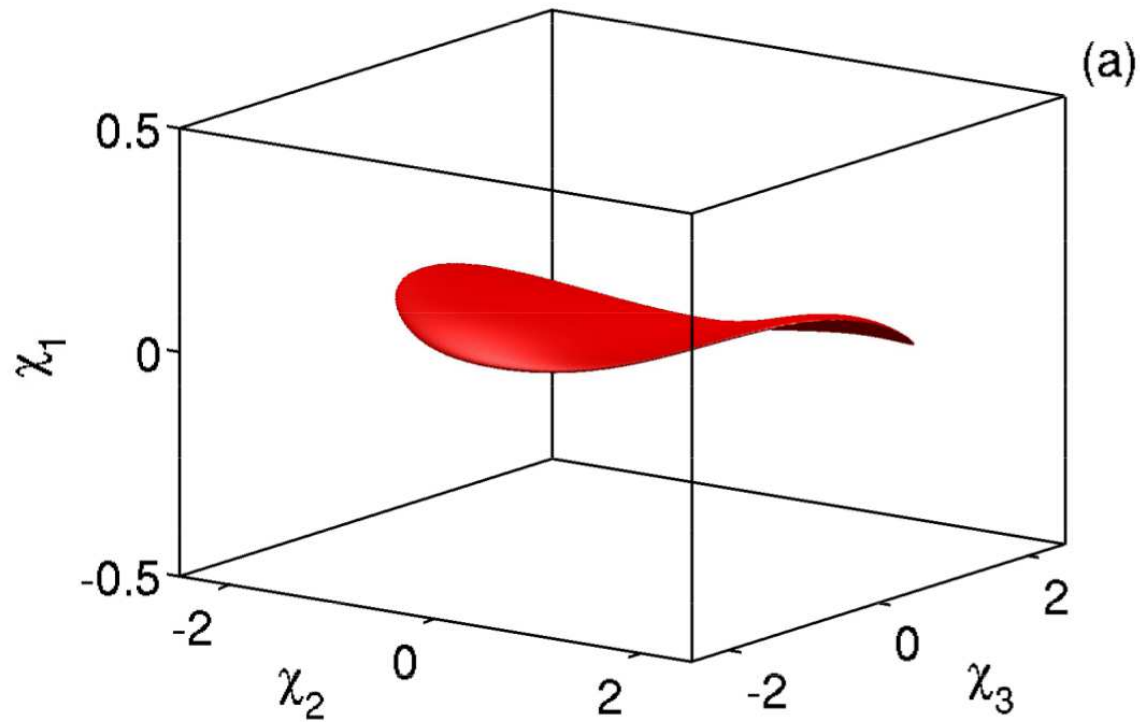
Evolution of local vorticity maximums (logarithmic vertical scale). Green line shows the global maximum, dashed red line indicates the slope $\propto e^{t/T_\omega}$ with $T_\omega = 2$.
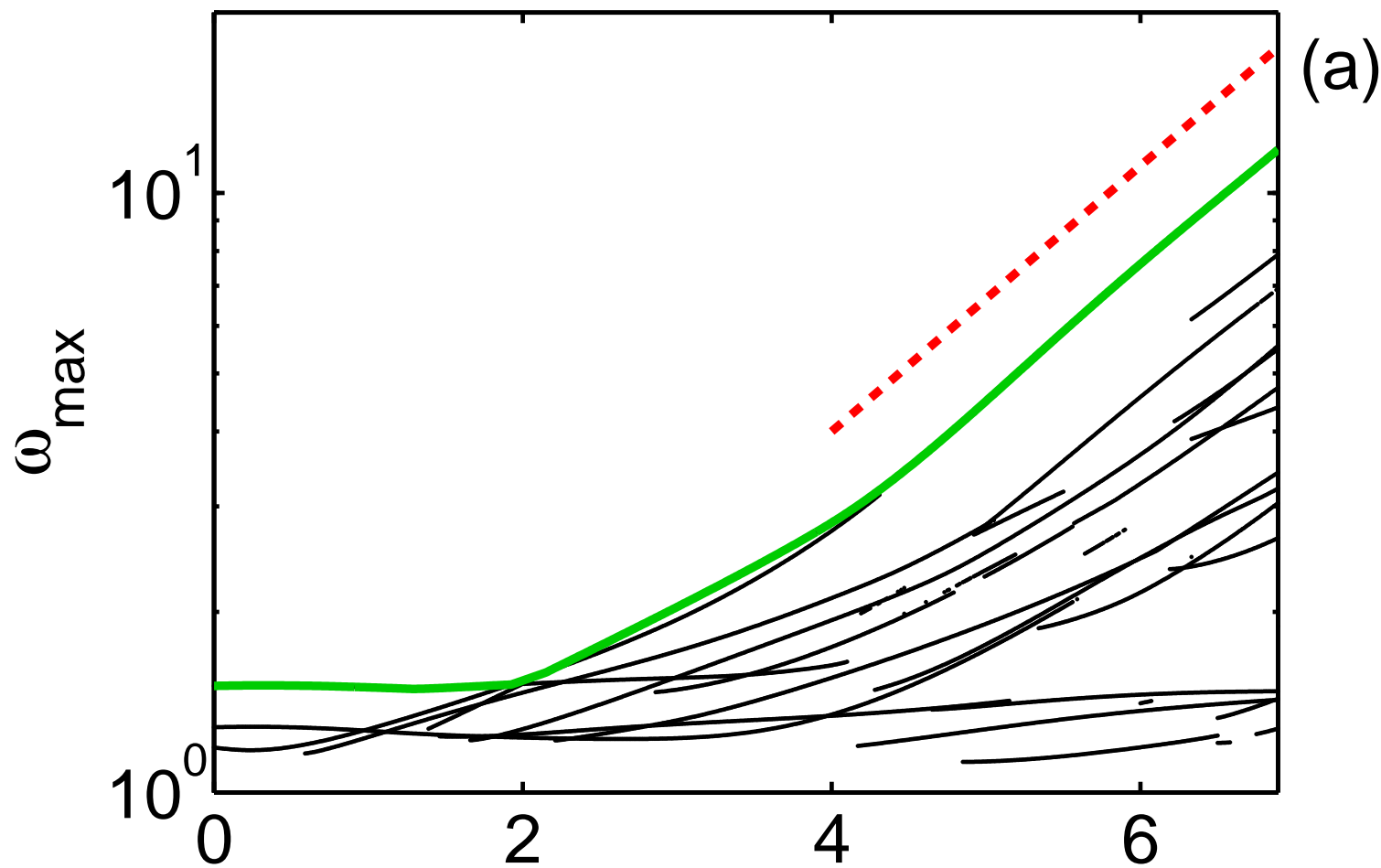
(a)

Evolution of characteristic spatial scales ℓ_1 (black), ℓ_2 (blue) and ℓ_3 (red) for the global vorticity maximum. Dashed red line indicates the slope $\propto e^{-t/T_\ell}$ with $T_\ell = 1.4$.
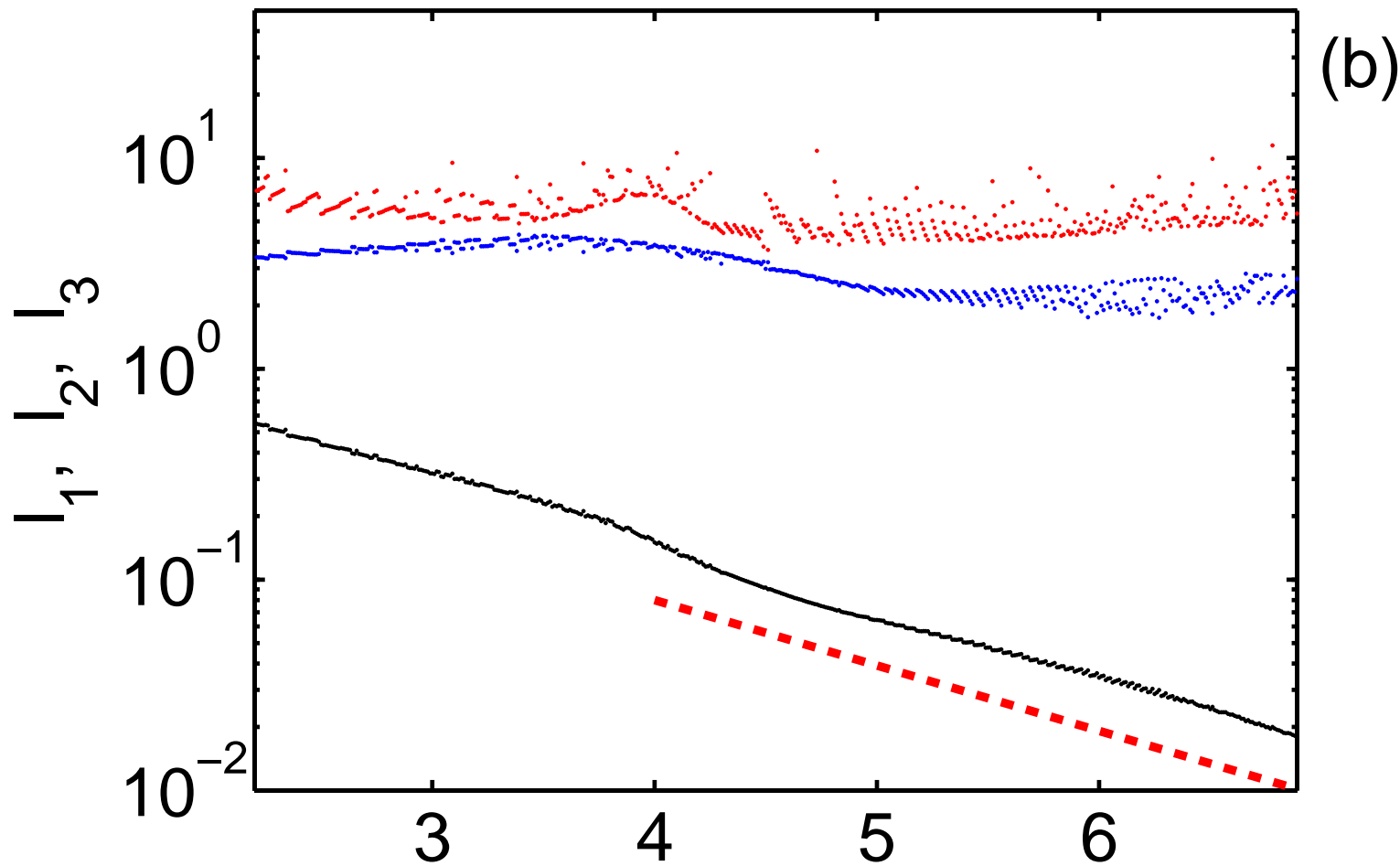
Numerical experiment, direct code, 1st IC

Vorticity local maximums $\omega_{\max}(t)$ vs. lengths $\ell_1(t)$ during the evolution of the pancake structures. Green line shows the global maximum, red circles mark local maximums at the final time. Dashed red line indicates the power-law $\omega_{\max} \propto \ell_1^{-2/3}$.

(d)
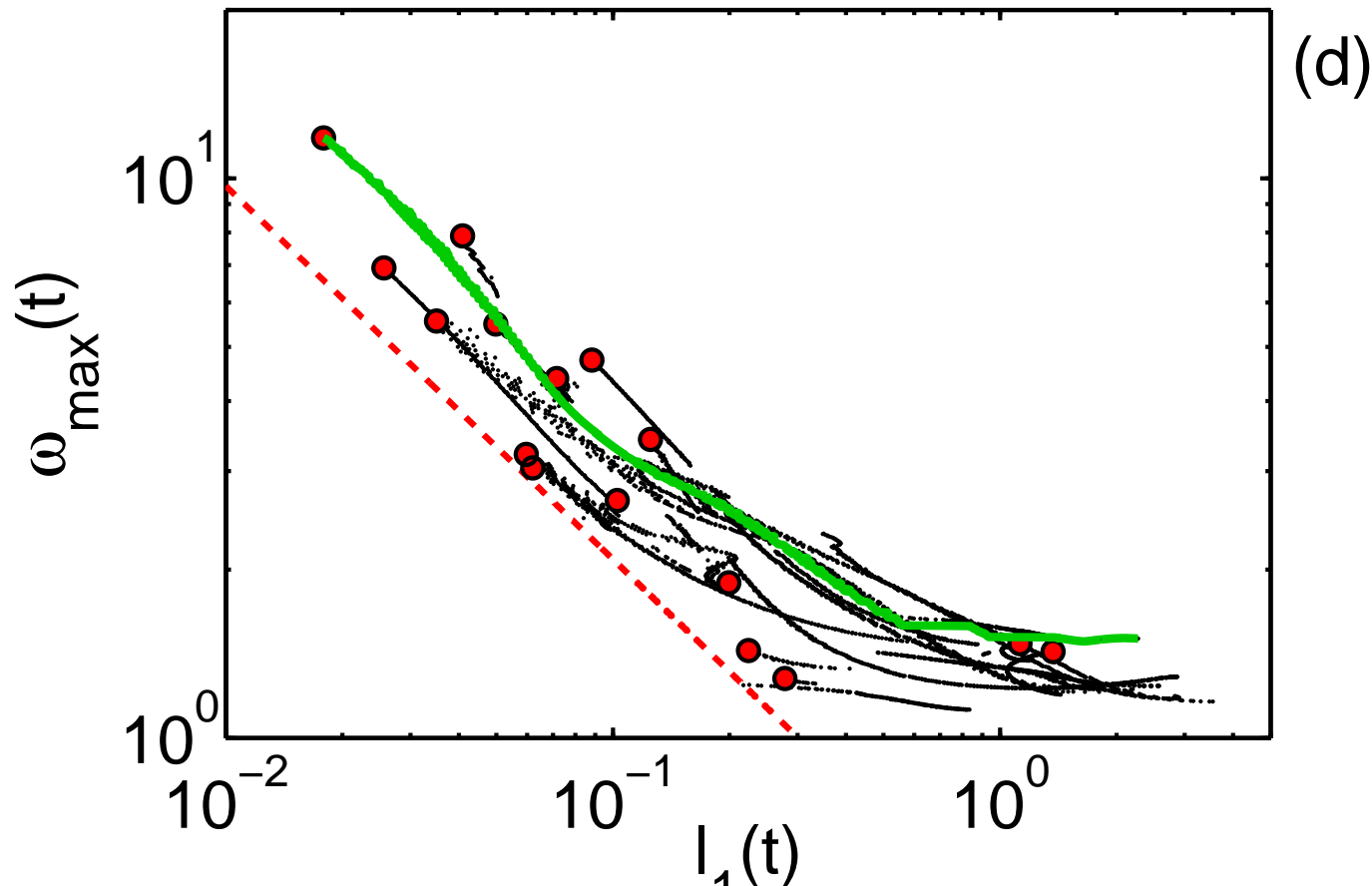
Evolution of the global vorticity maximum (logarithmic vertical scale). Dashed red line indicates the slope $\propto e^{t/T_\omega}$ with $T_\omega = 2.7$.

(a)
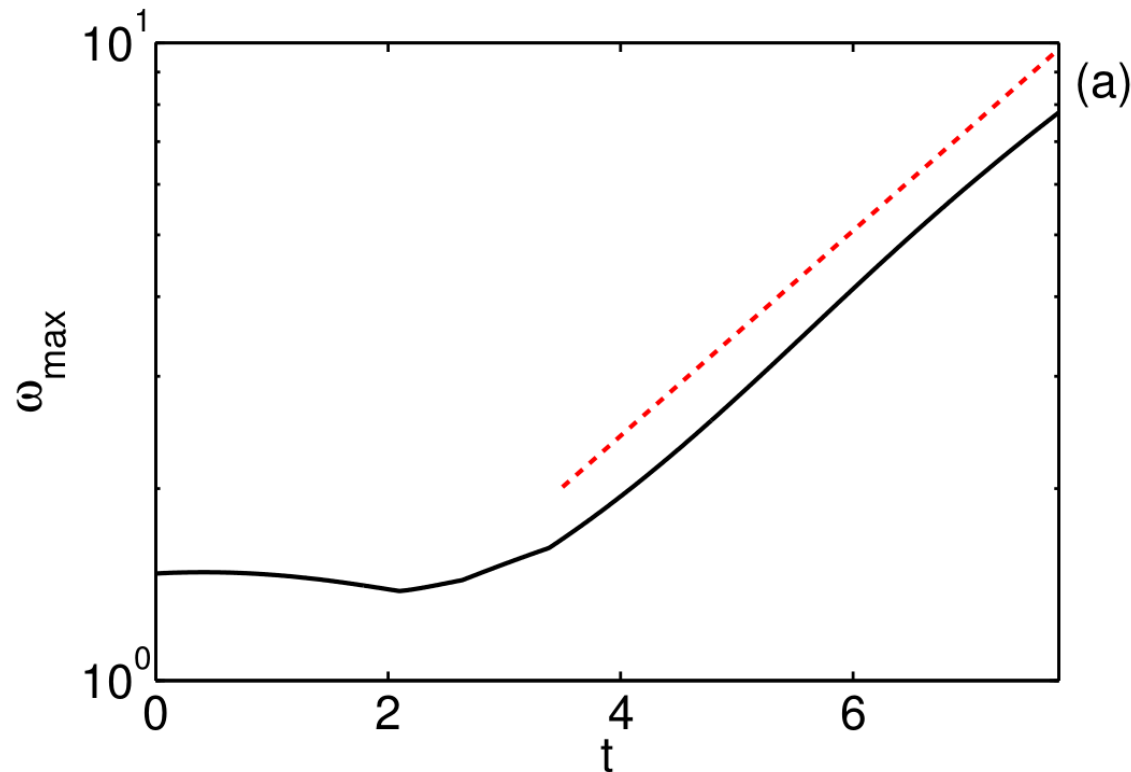
Numerical experiment: direct code, 2nd IC

Evolution of characteristic spatial scales ℓ_1 (black), ℓ_2 (blue) and ℓ_3 (red) for the local vorticity maximum, which appeared at $t = 2.36$ and became the global maximum at the end of the direct simulation $t = 7.77$. Dashed red line indicates the slope $\propto e^{-t/T_\ell}$ with $T_\ell = 1.7$.
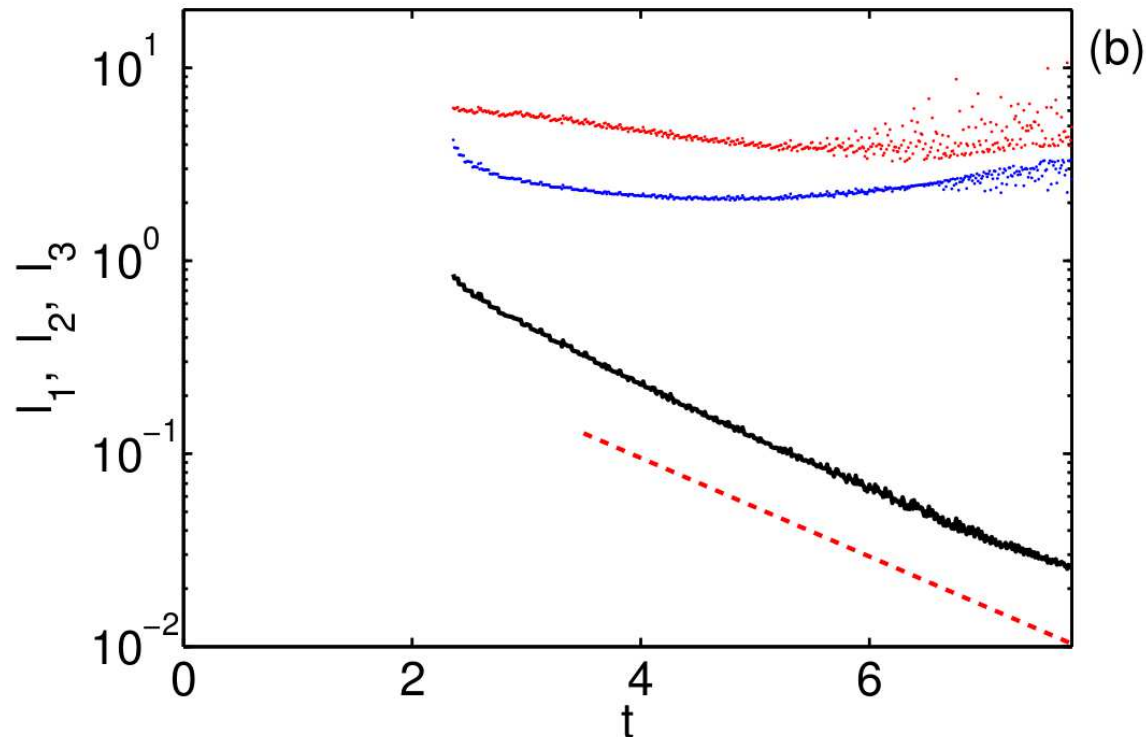
Numerical experiment: direct code, 2nd IC

Vorticity maximum $\omega_{\mathrm{max}}(t)$ vs. pancake thickness $\ell_1(t)$ during evolution of the pancake, which appeared at $t = 2.36$ and yielded the global vorticity maximum at the end of the direct simulation. Red circle marks the vorticity maximum at $t = 7.77$, dashed red line indicates the power-law scaling $\omega_{\mathrm{max}} \propto \ell_1^{-2/3}$.
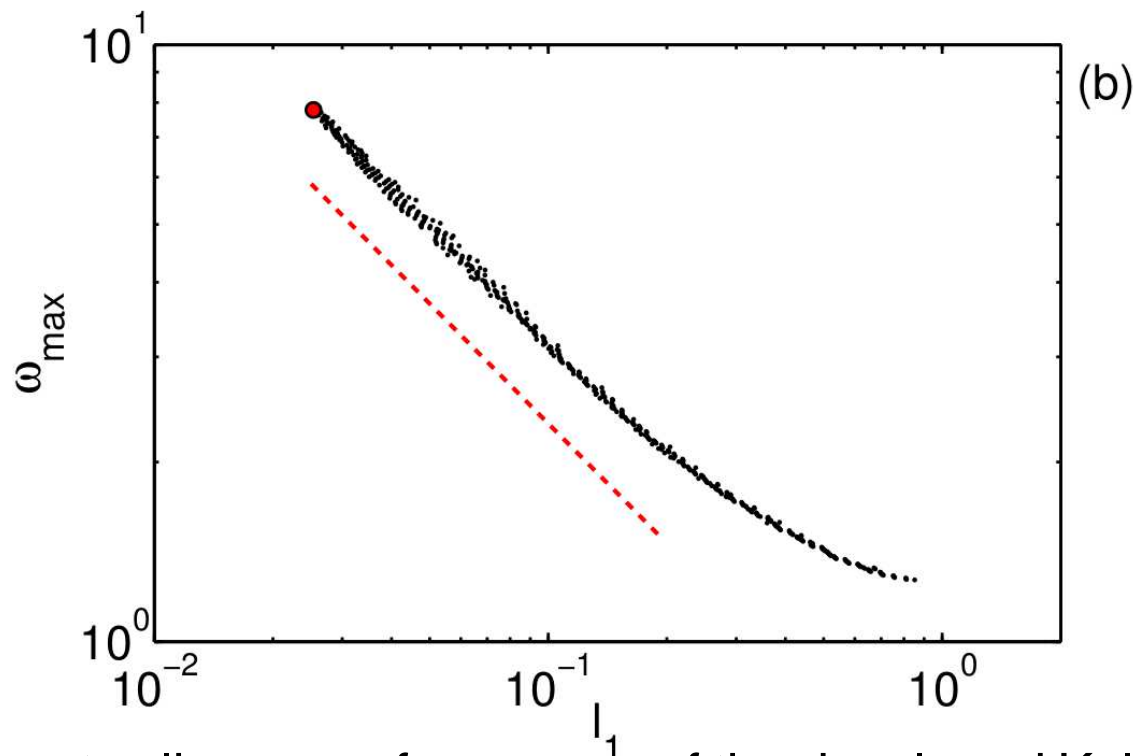
Components of the vorticity vector $\omega = (\omega_1, \omega_2, \omega_3)$ as functions of a_1 perpendicular to the pancake, at the final time.
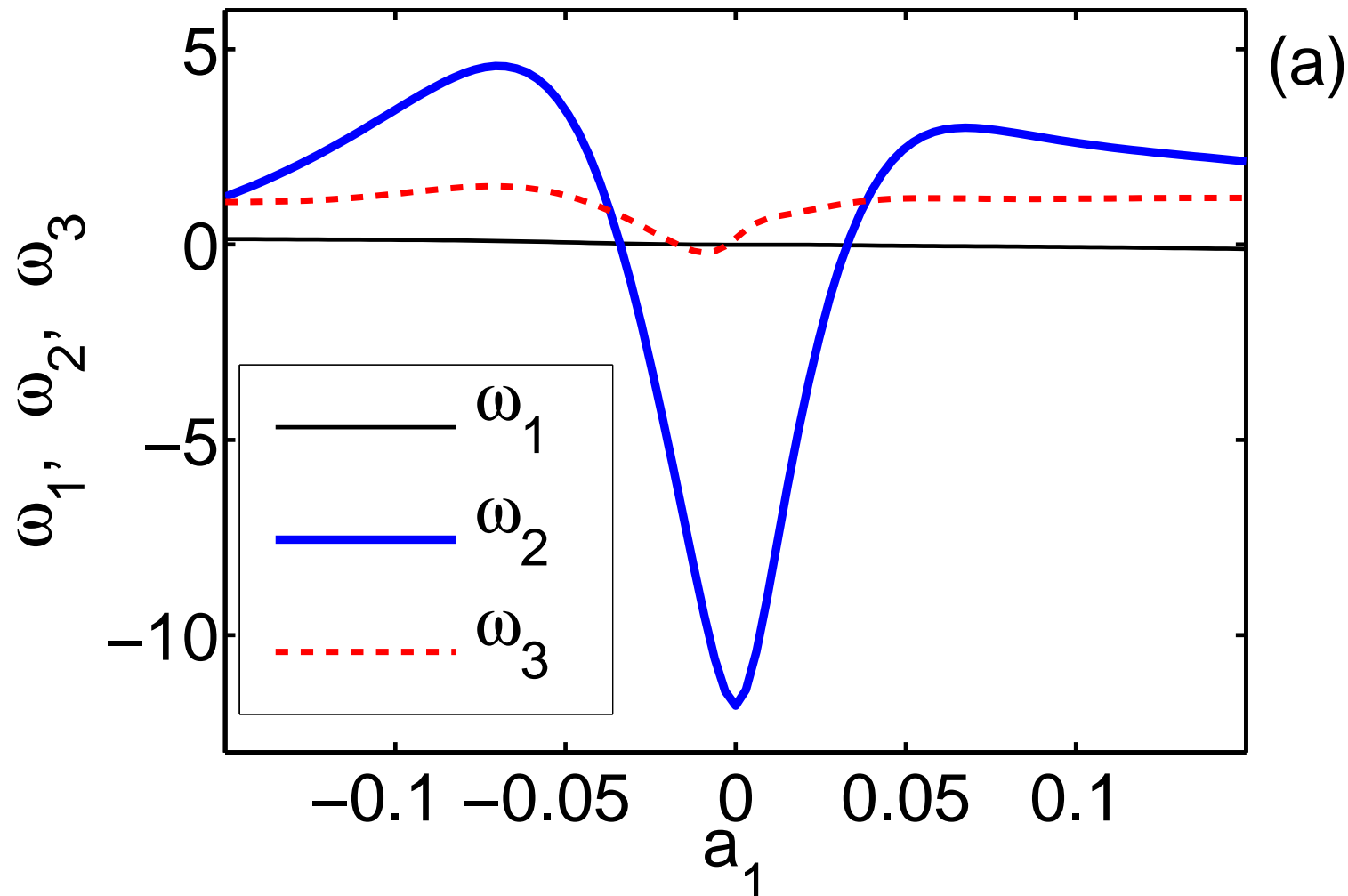
Numerical experiment, direct code, 1st IC

Vorticity component $\omega_2/\omega_{\max}$ vs. coordinate a_1/ℓ_1 at different times, demonstrating the self-similarity from $\ell_1(5) = 0.064$ to $\ell_1(6.89) = 0.018$.
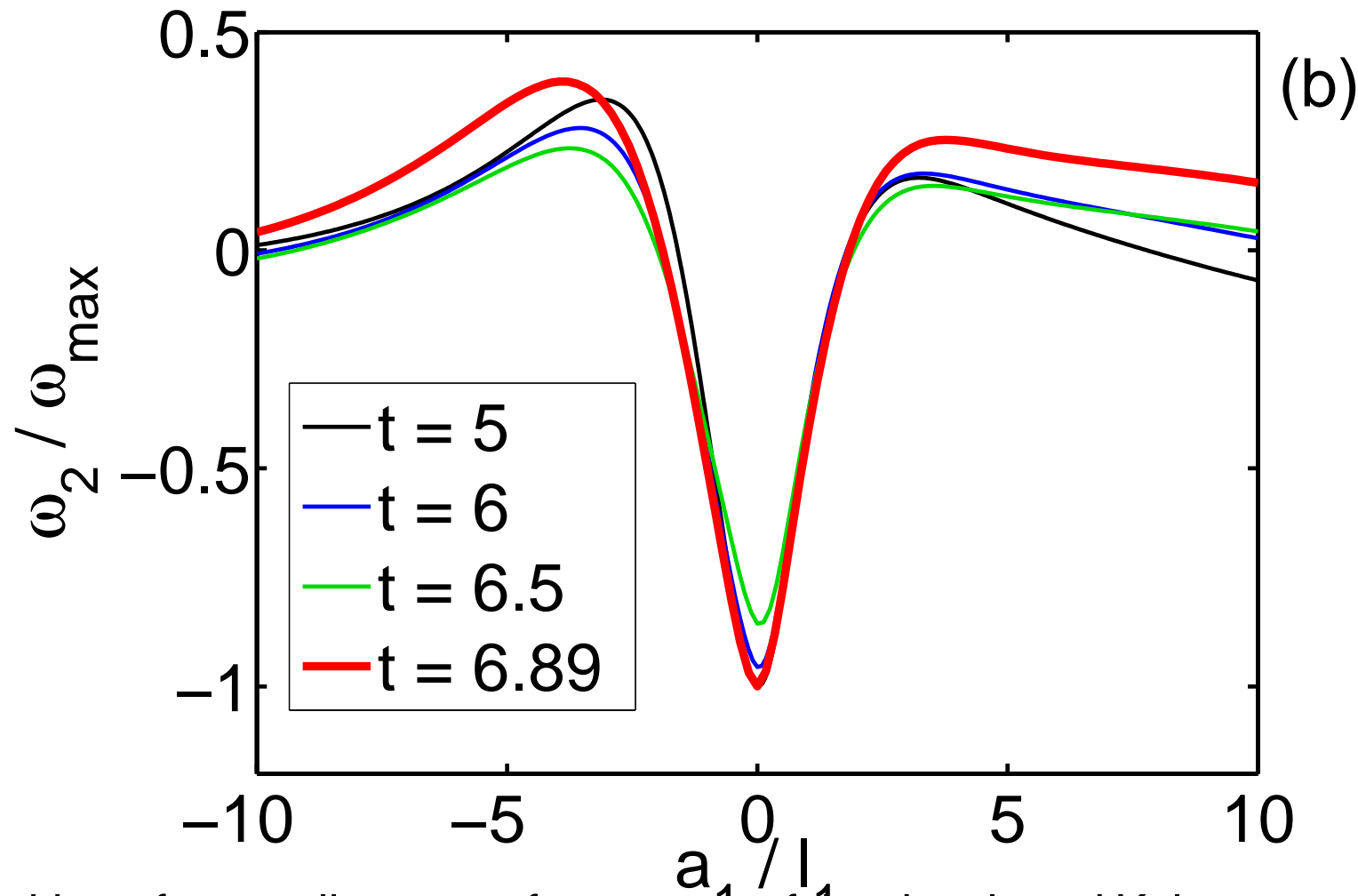
Evolution of local Jacobian minimums (logarithmic vertical scale). Dashed red line indicates the exponential slope $J_{\min} \propto e^{-t/T_J}$ with characteristic time $T_J = 2.9$.
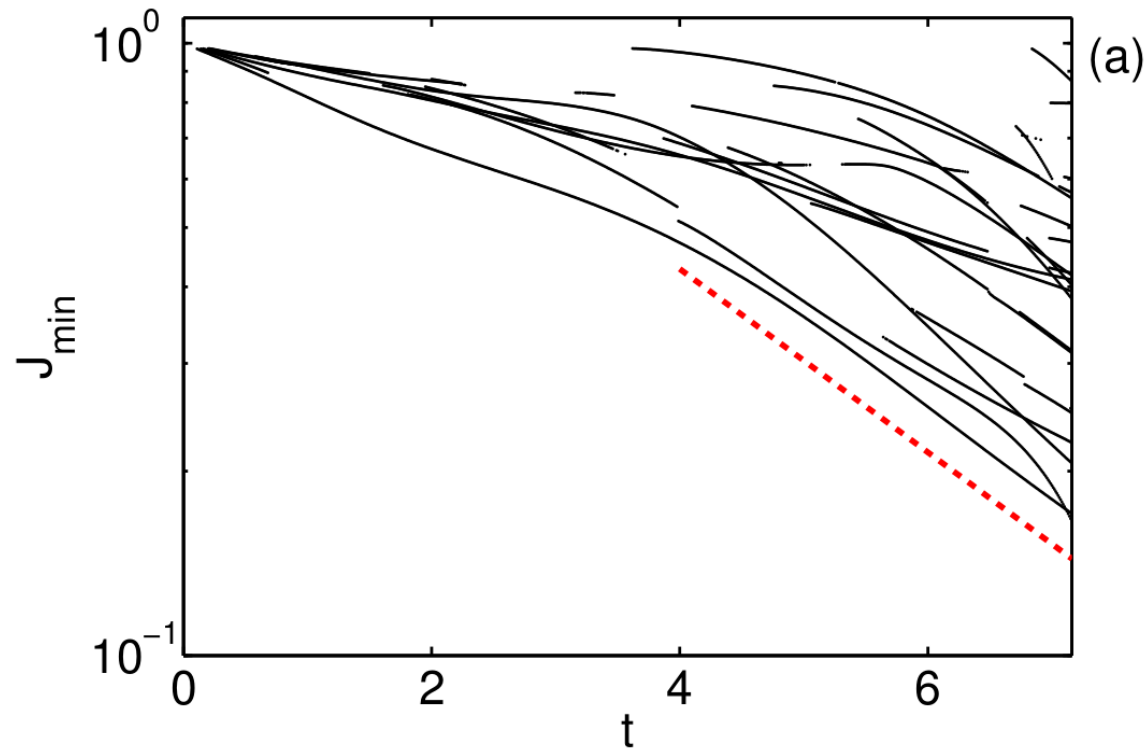
Numerical experiment: direct code, 2nd IC

Evolution of logarithmic derivative $d/dt \left[\log \omega_{\max}\right]$ (black) and divergence of velocity component normal to vorticity $-\mathrm{div}\,\mathbf{v}_n$ (red), at the point of global vorticity maximum. Dash-dot black shows the inverse characteristic time $1/T_\omega$, $T_\omega \approx 2.7$, for the growth of maximal vorticity, $\omega_{\max} \propto e^{t/T_\omega}$.
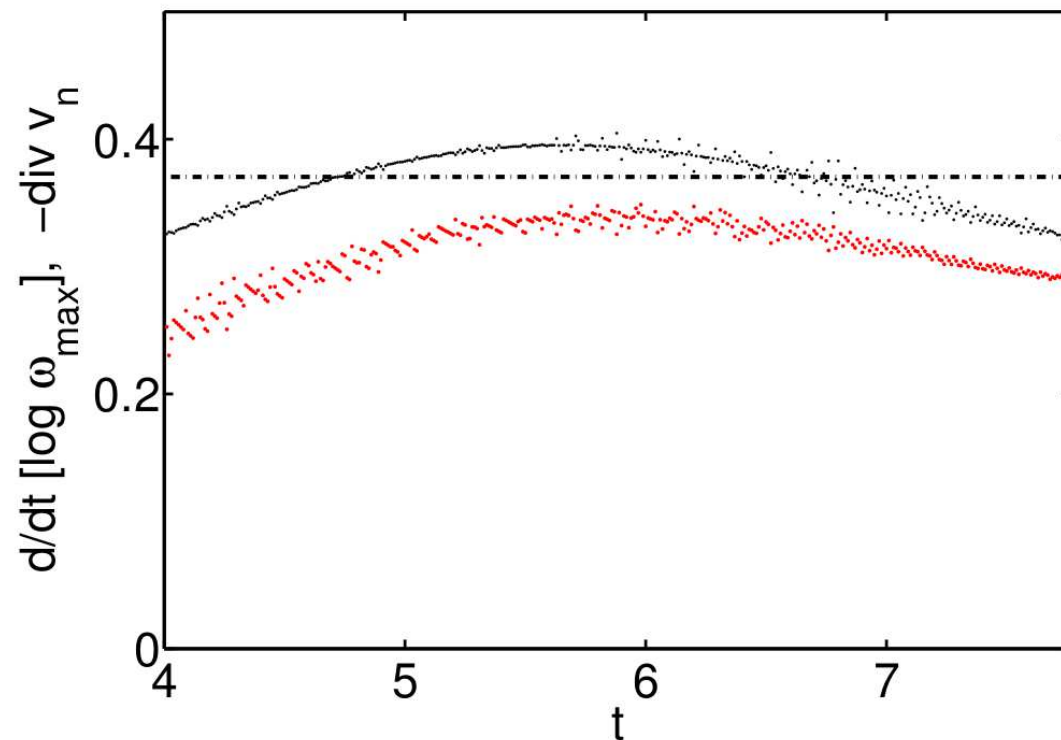
Evolution of eigenvalues μ_j, $j = 1, 2, 3$, of the Jacobi matrix for the local Jacobian minimum that appeared at $t = 2.16$ and became the global Jacobian minimum at the end of the VLR simulation $t = 7.1$.
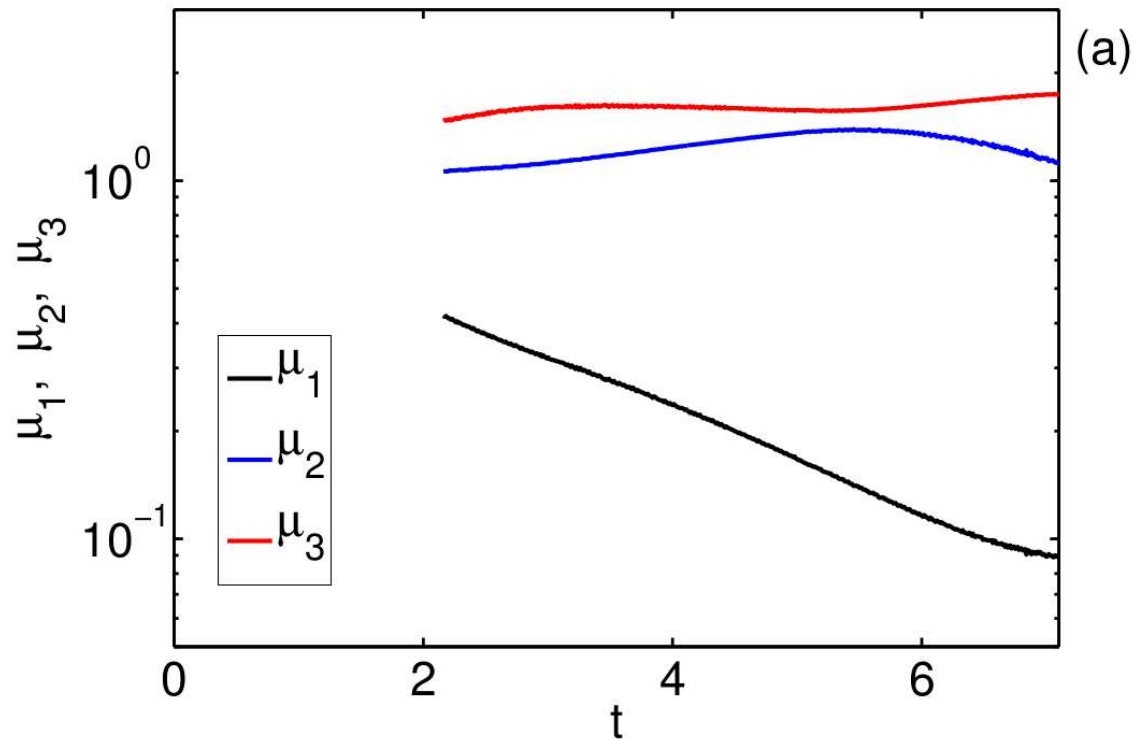
Evolution of $\gamma_{ij} = (1/2)\, \partial^2 J/\partial a_i \partial a_j$ components for this local minimum of Jacobian.
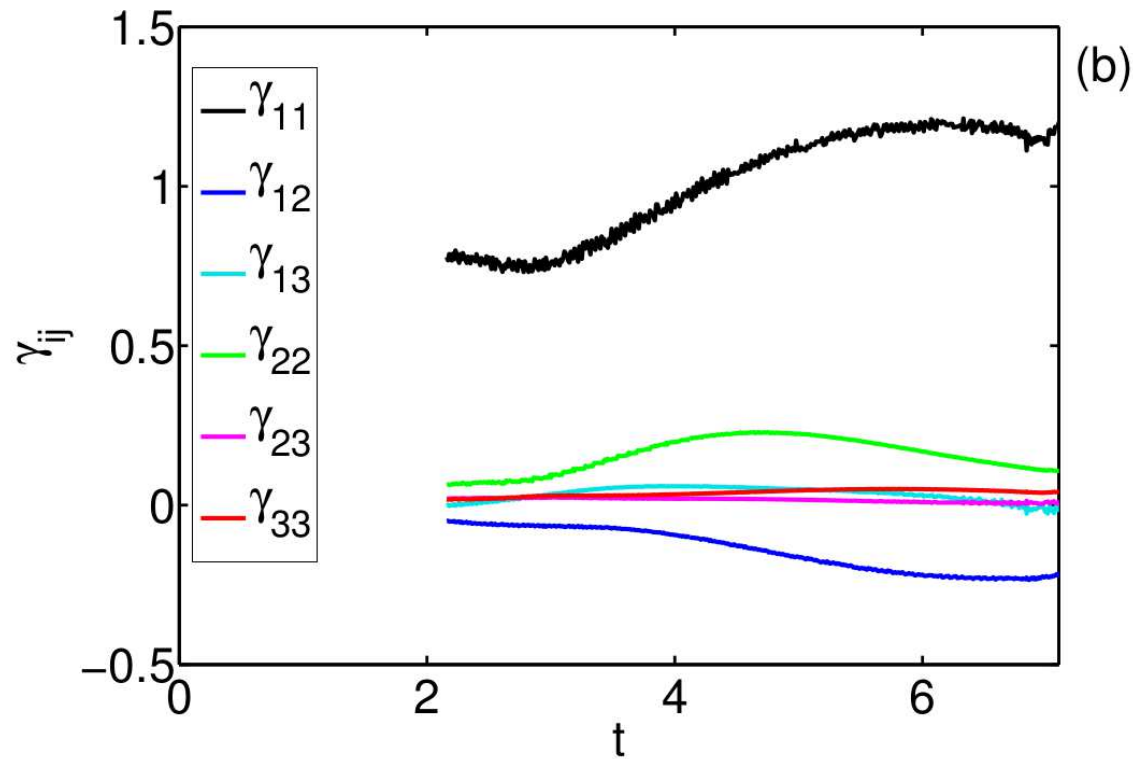
D. Agafontsev. Exact solution of 3D Euler

Exact solution of 3D Euler equations with scalings
$\omega_{\max}(t) \propto e^{t/T_\omega}$ and $\ell_1(t) \propto e^{-t/T_\ell}$:

$$
\begin{aligned}
v_1 &= -a_1/T_\ell, \\
v_2 &= a_2/T_\omega, \\
v_3 &= \omega_{\max}\ell_1\, f(a_1/\ell_1) + [1/T_\ell - 1/T_\omega]a_3, \\
p &= -\frac{a_1^2}{2T_\ell^2} - \frac{a_2^2}{2T_\omega^2} - \frac{a_3^2}{2}[1/T_\ell - 1/T_\omega]^2
\end{aligned}
$$

$$
\omega_1 = \omega_3 = 0, \quad \omega_2 = -\omega_{\max}f'(a_1/\ell_1)\,.
$$

Here f is an arbitrary function and ratio T_ℓ/T_ω is also
arbitrary, i.e. here we have a big degeneracy. Comparison of
this solution with the simulations gives a good agreement at
the pancake region.

Numerical experiment

- By means of the VLR scheme it was demonstrated decreasing of the Jacobian. This means that formation of the pancake structures can be considered as folding (breaking) of the vorticity lines.

- By use of the direct integration we found that at the maximal vorticity point

$$\frac{1}{\omega_{max}} \frac{d\omega_{max}}{dt} \simeq -\text{div } \mathbf{v_n}.$$

This means that the main contribution into the vorticity maximum comes from the denominator,

$$\omega(\mathbf{r}, t) = \frac{(\omega_0(\mathbf{a}) \cdot \nabla_a)\mathbf{r}(\mathbf{a}, t)}{J(\mathbf{a}, t)}.$$

Numerical experiment

JETS: Isosurface $|\tilde{\omega}(\mathbf{k})| = 0.2$ of the normalized vorticity field in $\mathbf{k}$- space at the final time. Solid lines show maximal $\mathbf{k}$-vectors for all jets (normalized by $1/\ell_1$).
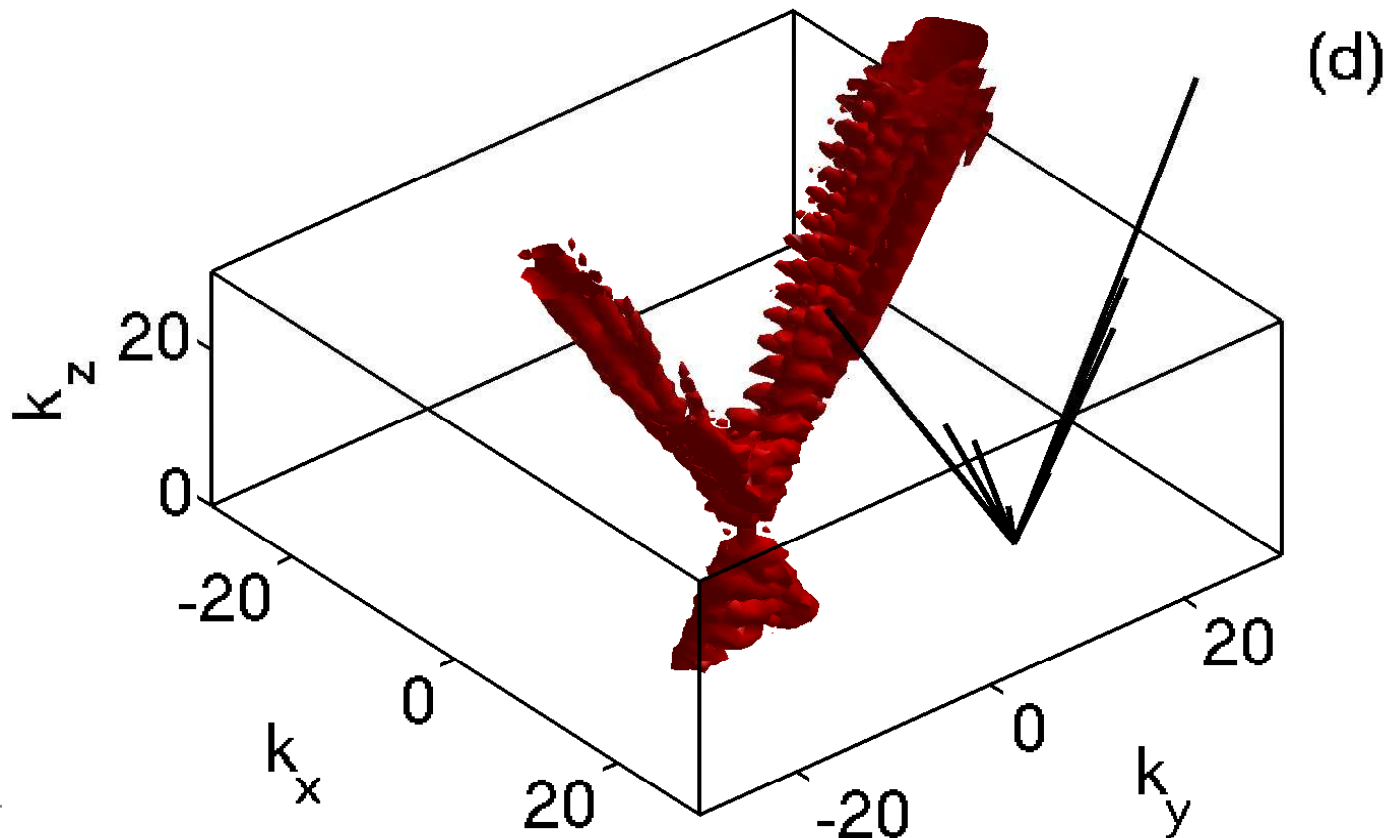
Energy spectrum at different times demonstrating the
Kolmogorov power-law.
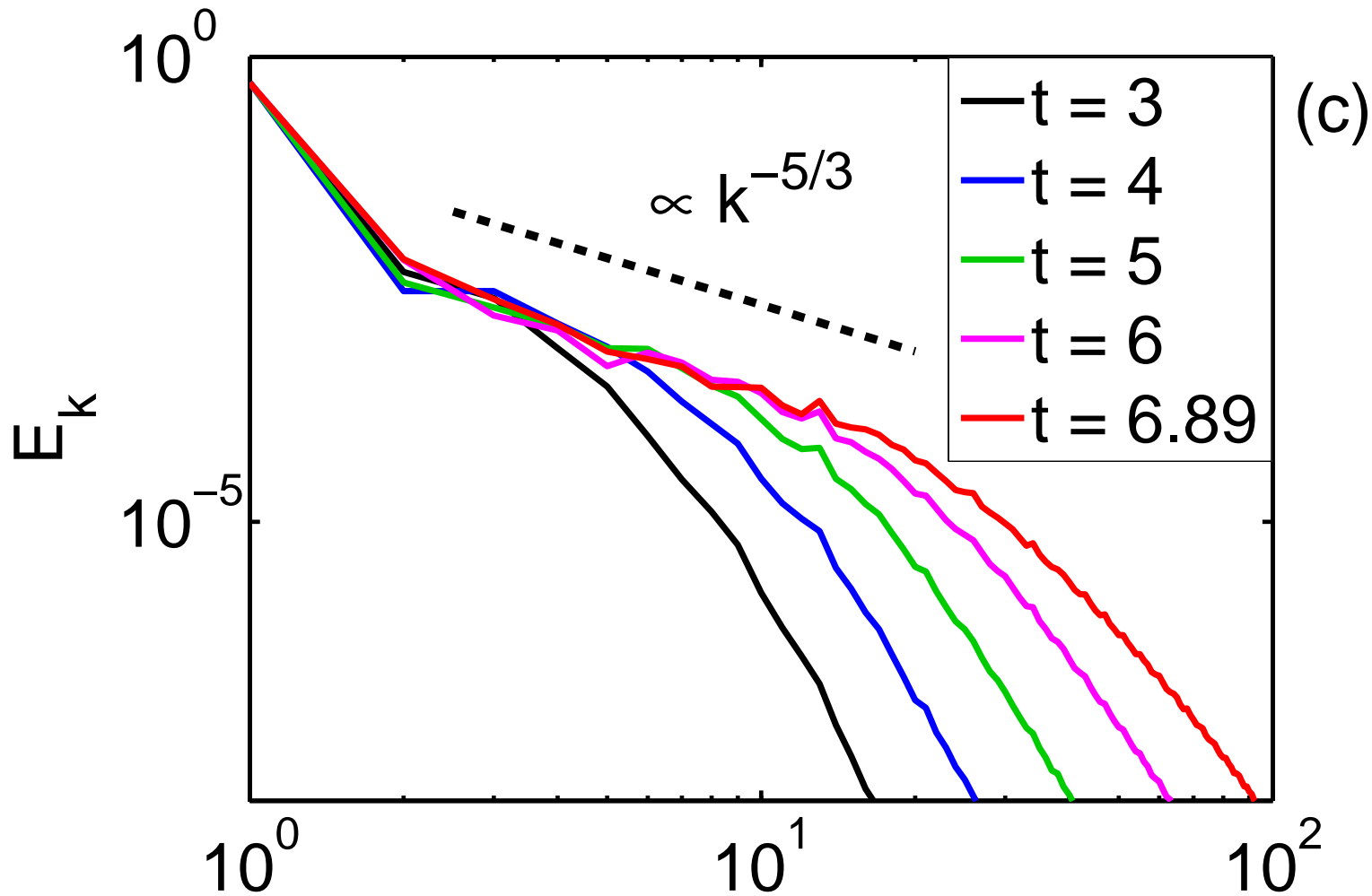
2D turbulence

- Following Kolmogorov (1941), each integral in its own transparency region must provide the corresponding Kolmogorov spectrum.

- For 2D HD turbulence, the energy conservation provides the Kolmogorov spectrum $E_k \sim P^{2/3} k^{-5/3}$ with energy flux P directed to small k (inverse cascade).

- The enstrophy provides Kraichnan spectrum(1967) with enstrophy flux directed to large k (direct cascade): $E_k \sim \eta^{2/3} k^{-3}$ where η is the enstrophy flux.

2D turbulence

- (1971) Saffman spectrum, $E_k \sim k^{-4}$, appears due to vorticity (quasi-)discontinuities which were observed in many numerical experiments (Lilly, 1971; Deem, Zabusky, 1978; McWilliams, 1984; Kida, 1985; Brachet, Meneguzzi, & Sulem, 1986; Okhitani, 1991).

- The Saffman idea was developed by K., Naulin, Nielsen, and Rasmussen, 2007. If one assumes, that vorticity ω undergoes jumps with widths $\delta \ll L$, the characteristic scale, then it easy to get that the spectrum generated by such jumps should be $\sim k^{-3}$. Each jump gives the jet-like distribution with angular width $\theta \sim (kL)^{-1}$. In a pure isotropic case we arrive at the Saffman spectrum. Thus, only strong angular dependence can provide the Kraichnan-type spectrum.

Tendency to breaking in 2D turbulence

Formation of vorticity quasi-shocks can be understood if within the Euler equation one introduces the divergence-free vector $\mathbf{B}$ (di-vorticity),

$$B_x = \frac{\partial \omega}{\partial y}, \qquad B_y = -\frac{\partial \omega}{\partial x}.$$

where $\mathbf{B}$ obeys the equation

$$\frac{\partial \mathbf{B}}{\partial t} = \mathrm{rot}\,[\mathbf{v} \times \mathbf{B}].$$

This vector field (the di-vorticity) is frosen-in, changes due to the velocity component $\mathbf{v_n}$, normal to $\mathbf{B}$. It is easily seen also that this vector is tangent to the line $\omega(x,y) = \mathsf{const}$.

Tendency to breaking in 2D turbulence

In terms of the substantial derivative Eq. for di-vorticity can be rewritten as

$$\frac{d\mathbf{B}}{dt} = (\mathbf{B} \cdot \nabla)\mathbf{v} \equiv \frac{1}{2}\left[\omega\hat{z} \times \mathbf{B}\right] + \hat{S}\mathbf{B}.$$

The r.h.s. describes the rotation of the vector $\mathbf{B}$ and stretching of the di-vorticity lines where

$$\hat{S}_{ik} = \frac{1}{2}\left(\frac{\partial v_k}{\partial x_i} + \frac{\partial v_i}{\partial x_k}\right)$$

is the stress tensor. The divorticity length $|\mathbf{B}|$ will locally increase when

$$\frac{1}{2}\frac{d\mathbf{B^2}}{dt} = (\mathbf{B} \cdot \hat{S}\mathbf{B}) > 0.$$

Tendency to breaking in 2D turbulence

By introducing new trajectories,

$$\frac{d\mathbf{r}}{dt} = \mathbf{v}_n(\mathbf{r}, t); \quad \mathbf{r}|_{t=0} = \mathbf{a},$$

$\mathbf{B}$ is expressed through the mapping $\mathbf{r} = \mathbf{r}(\mathbf{a}, t)$ and its Jacobian J (analog of VLR, Kuznetsov & Ruban, 1998, Kuznetsov, 2002):

$$\mathbf{B}(\mathbf{r}, t) = \frac{(\mathbf{B}_0(\mathbf{a}) \cdot \nabla_a)\mathbf{r}(\mathbf{a}, t)}{J}$$

J is not fixed, i.e., the mapping is compressible, that is a reason of appearance of sharp gradients in 2D Euler (Kuznetsov, Naulin, Nielsen, and Rasmussen, 2007).

Numerical approach

- To support the above arguments and reveal the direct connection between the formation of the sharp vorticity gradients and the tail of the energy spectrum we have performed a numerical study of the evolution of decaying 2D turbulence.

- We solve numerically the vorticity equation with hyperviscosity

$$\frac{d\omega}{dt} = (-1)^{n+1}\mu_n \nabla^{2n}\omega, \quad \mu_n = 10^{-20}\left(\frac{2048}{N}\right)^{2n}, \quad n = 3$$

in a double periodic domain whose size is taken to be unity.

Numerical approach

- We use pseudospectral Fourier method and the 3rd order Runge–Kutta / Crank–Nicolson scheme. The FFTW library is used for computing the discrete Fast Fourier Transform.

- The computations have been performed on both the multiprocessor cluster (with MPI parallelization, up to 128 processors have been used) and the GPU cluster (using NVIDIA CUDA technology) at the Novosibirsk State University Computational Center.

- Spatial resolution is up to 8192×8192. The time scale corresponds to inverse maximal value of vorticity, ω_0^{-1}.

Numerical experiments for 2D decay turbulence

Initial distribution of ω; Distribution of vorticity at $t = 100$.
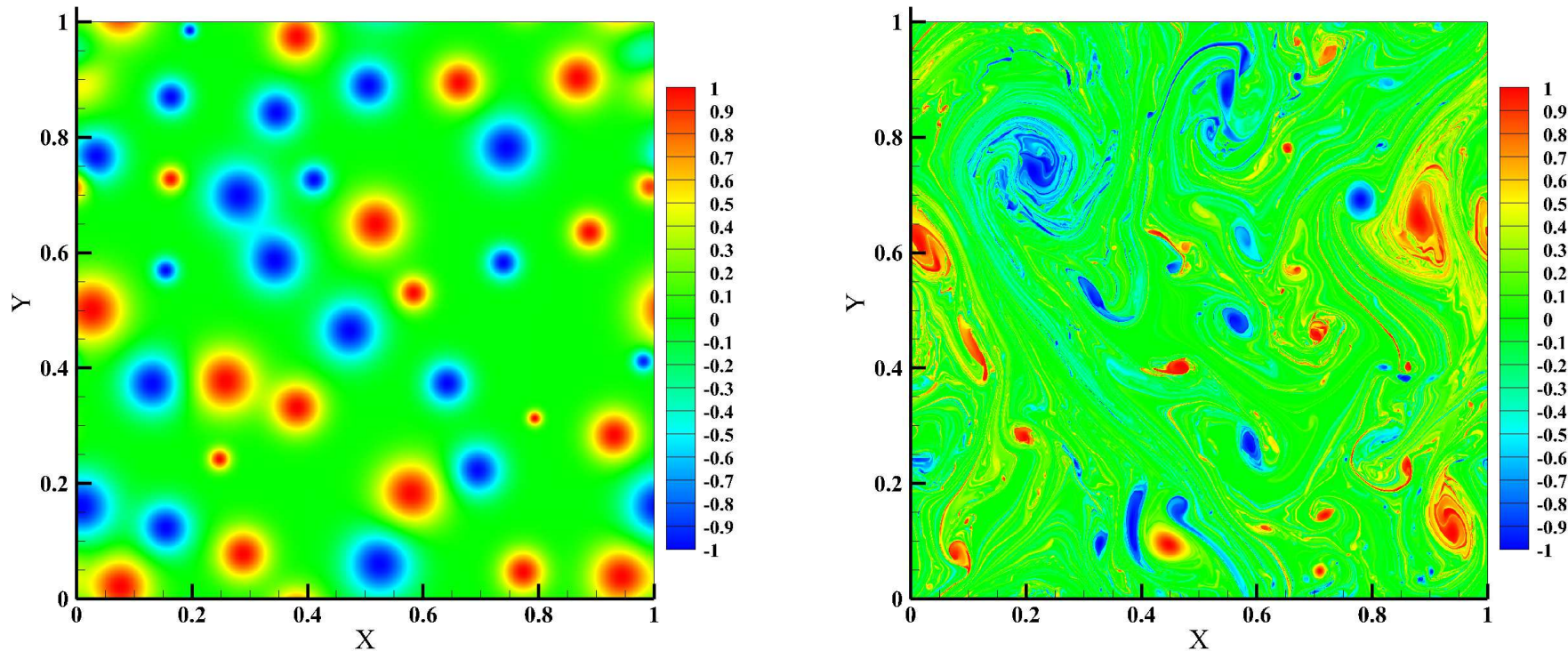
Vortices of both signs $N = 20$ with the Gaussian profile, a random radius and the unit maximum ω are randomly spaced within the domain with the zero total circulation.

Compensated energy spectrum at different times $k^3 E(k)$
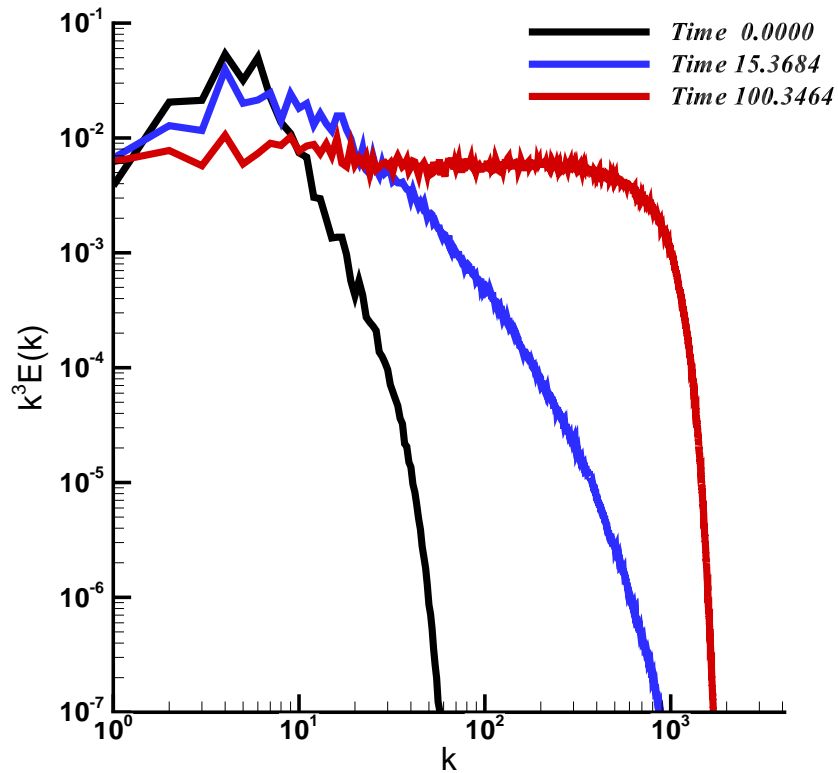
Numerical experiments for 2D decay turbulence

Distribution of $|\mathbf{B}|$ at $t = 100$
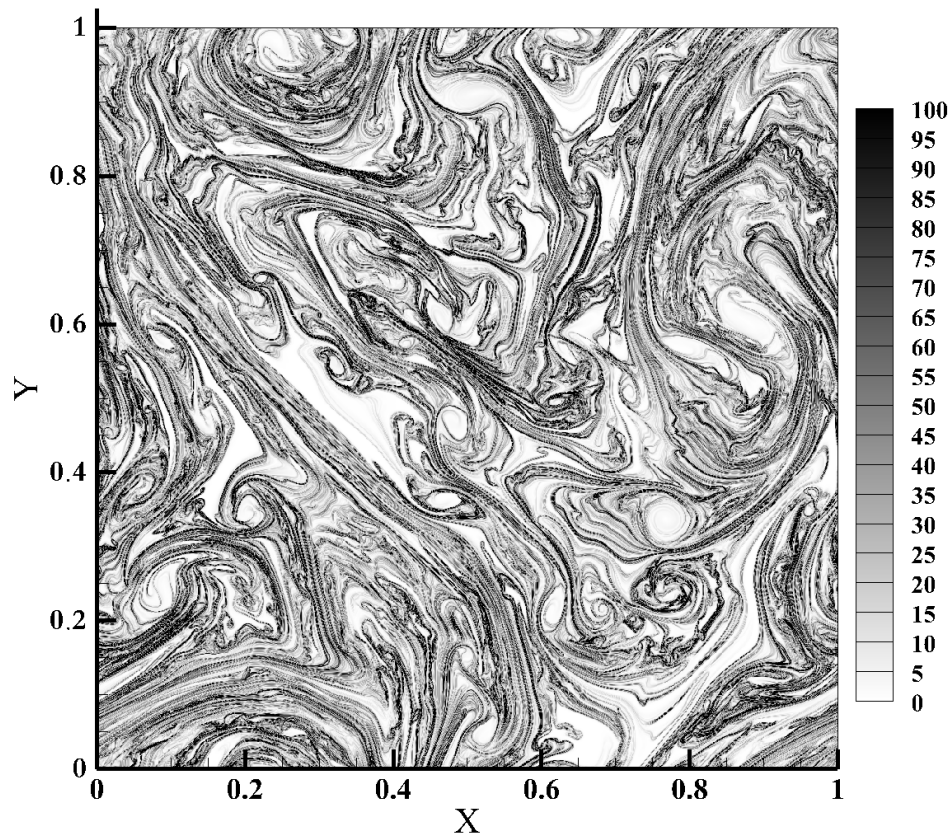
Numerical experiments for 2D decay turbulence

Dependence of B on x at $t = 75$.

Time 75.0338
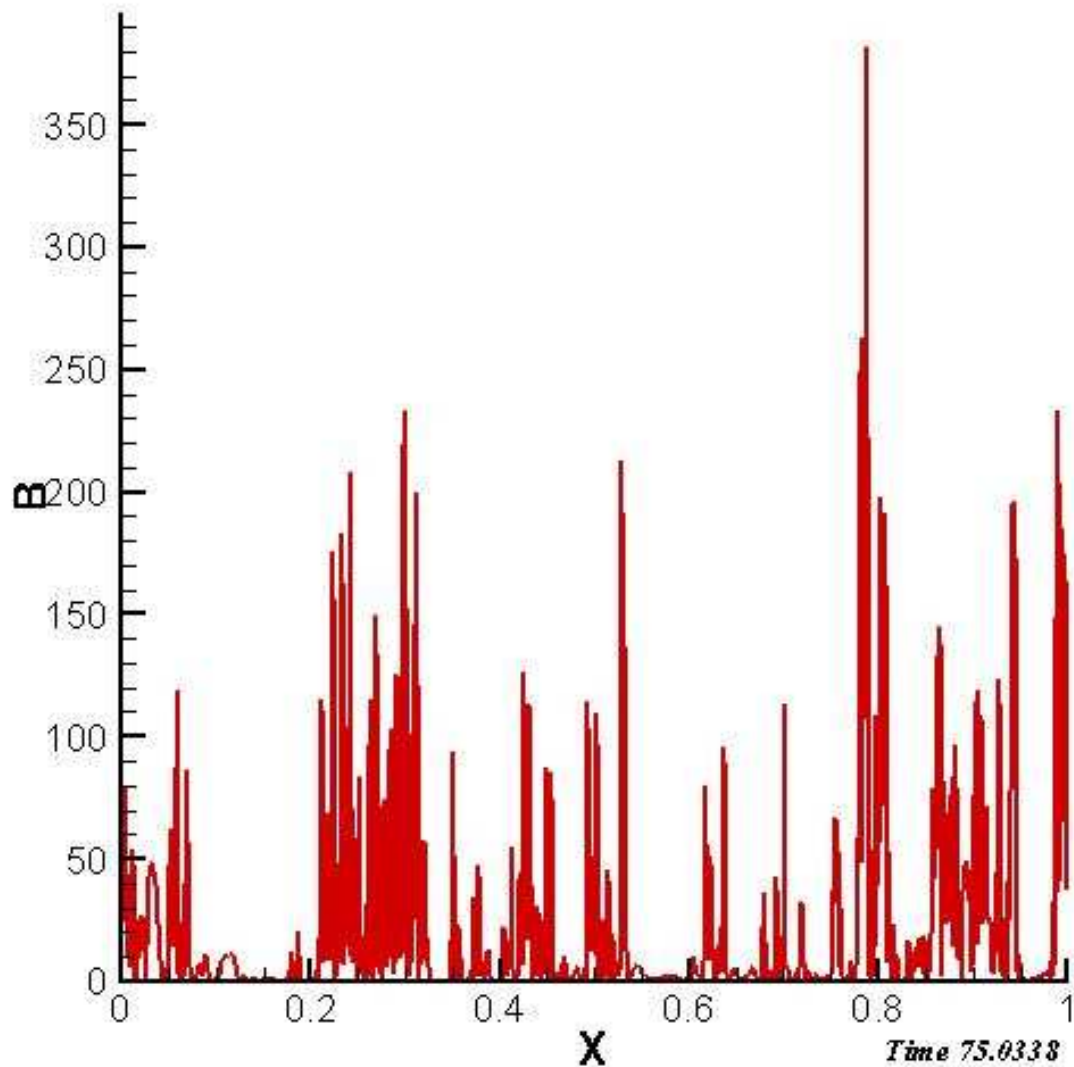
Numerical experiments for 2D decay turbulence

Growth of maximum of di-vorticity (logarithmic scale, the
straight line corresponds to the exponential growth)
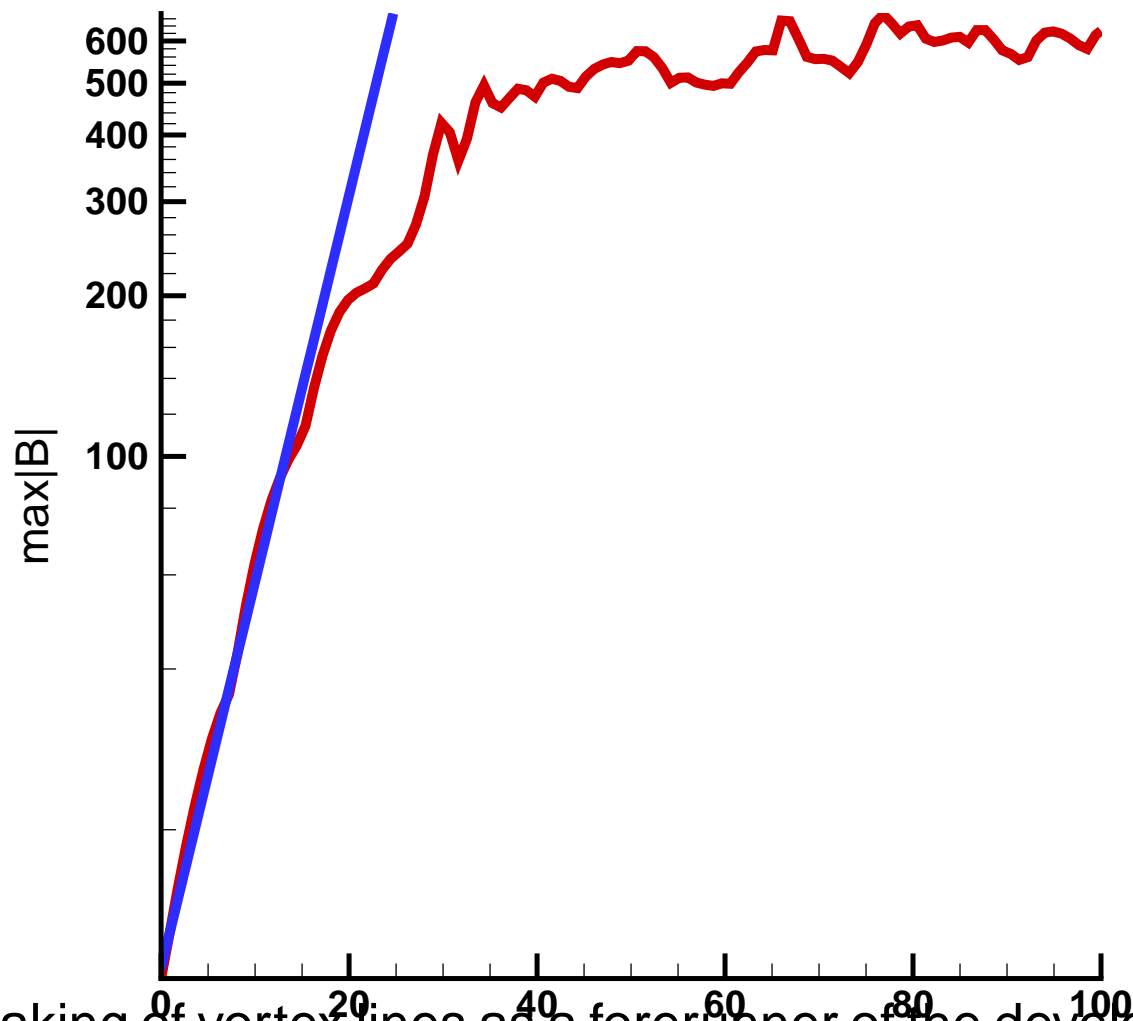
Numerical experiments for 2D decay turbulence

2D energy spectrum $k^4 \epsilon(k_x, k_y)$
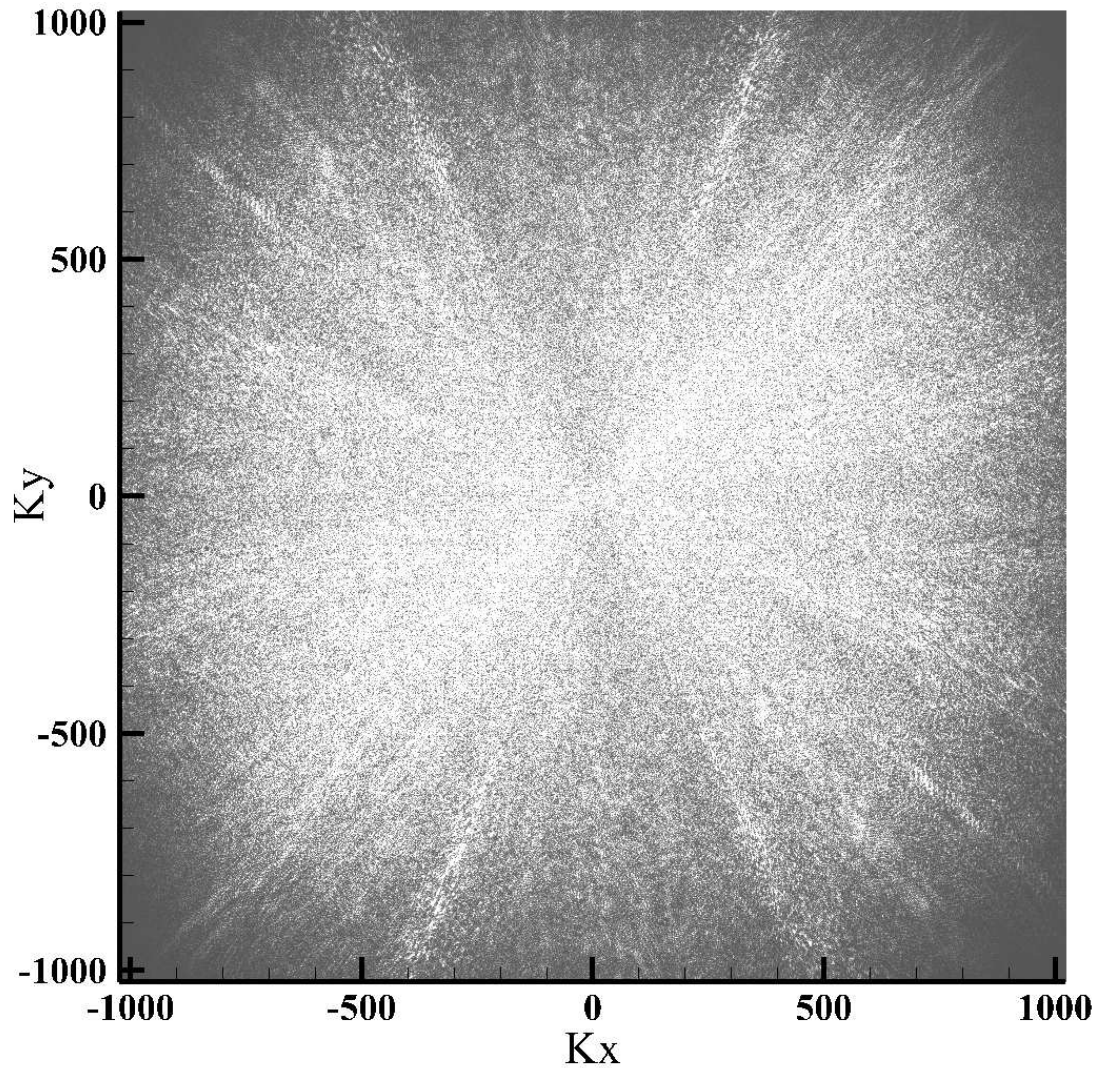
Numerical experiments for 2D decay turbulence

Filtered compensated spectra $k^3 \widetilde{E}(k)$ for different threshold values B_0
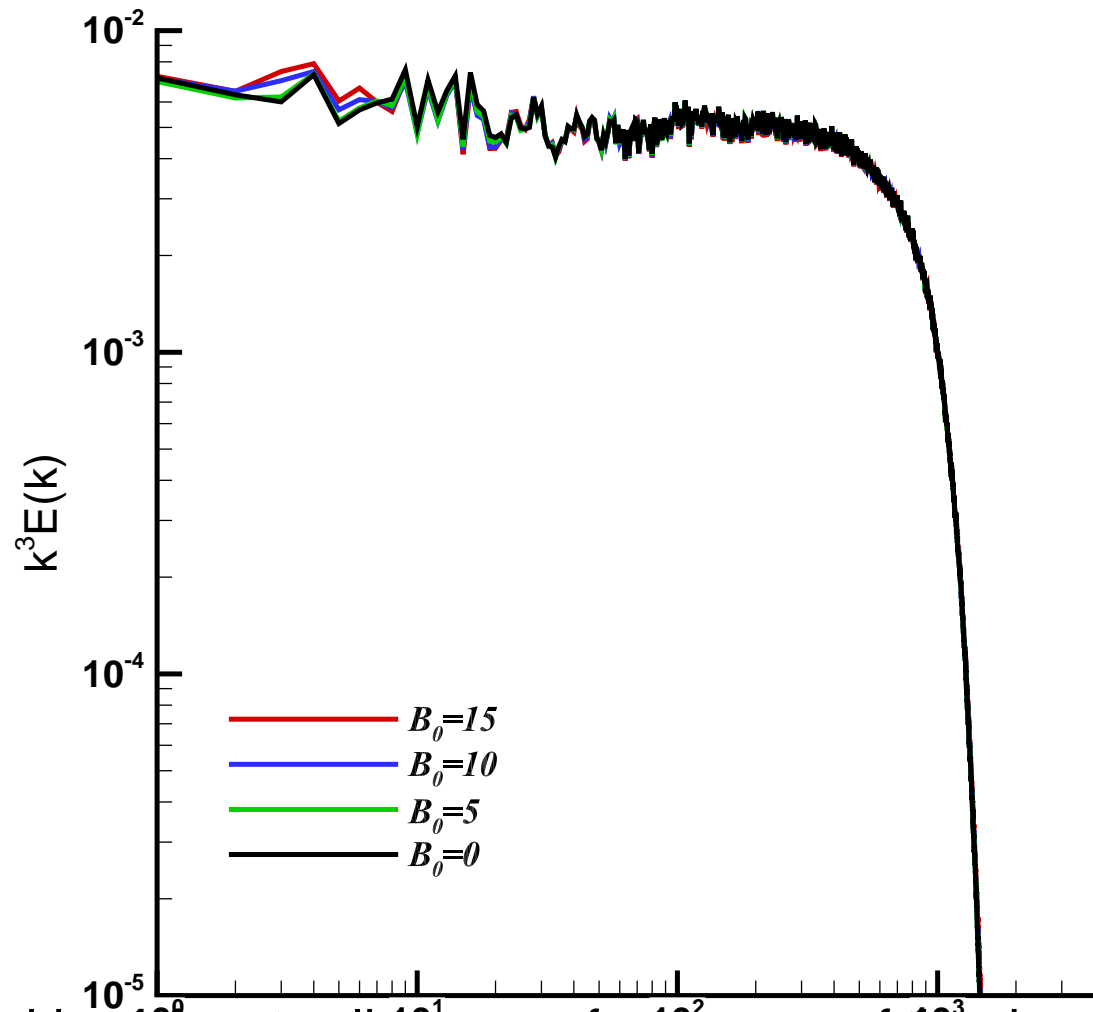
The velocity structure functions

$$S_n(R) = \left\langle \left[(\mathbf{v}(\mathbf{r}') - \mathbf{v}(\mathbf{r})) \cdot \frac{\mathbf{r}' - \mathbf{r}}{r' - r} \right]^n \right\rangle \sim R^{\zeta_n}.$$

Power law exponents ζ_n (local) as functions of R.
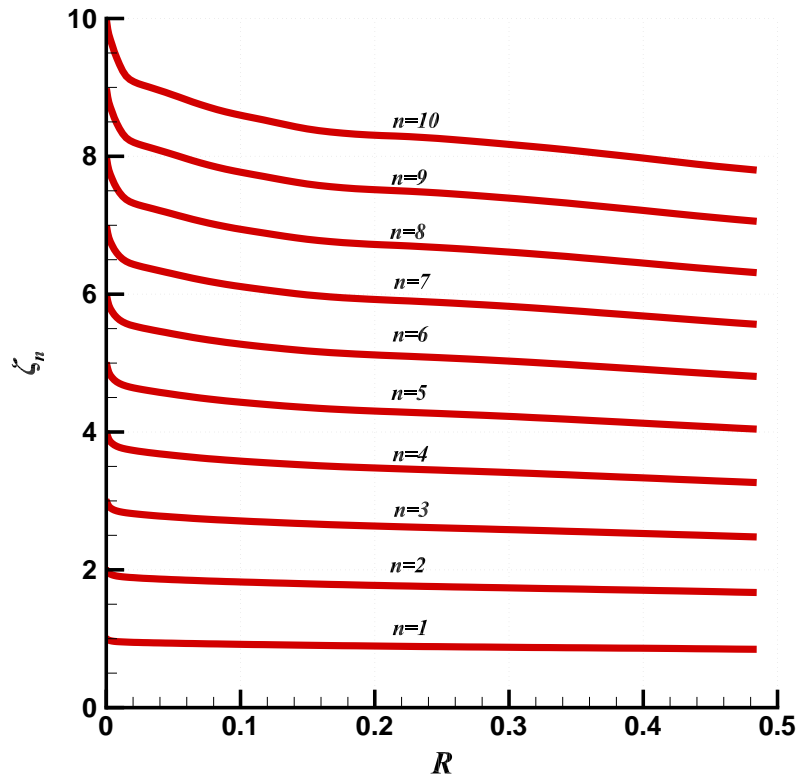
Correlation function $D(R) = \langle \delta u (\delta \omega)^2 \rangle$.
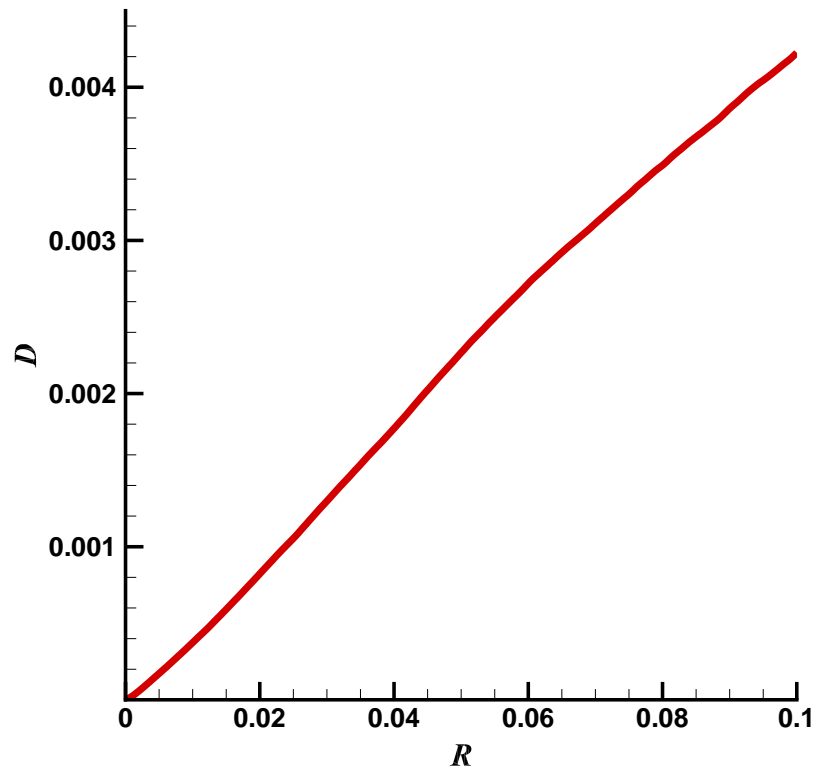
2D turbulence with pumping and viscous-type damping

We consider the two-dimensional Navier-Stokes equation for an incompressible flow in the vorticity formulation,

$$\frac{\partial \omega}{\partial t} + (\mathbf{u}\nabla)\omega = (\hat{\Gamma} + \hat{\gamma})\omega \qquad \text{with} \qquad \text{div}\,\mathbf{u} = 0,$$

where the Fourier transforms of $\hat{\Gamma}$

$$\Gamma_k = A\frac{(k^2 - b^2)(k^2 - a^2)}{k^2} \quad \text{at} \quad 0 \le k \le b,$$

$$\Gamma_k = 0 \quad \text{at} \quad k > b,$$

$b > a,\ A < 0$ and $\hat{\gamma}$ was taken in the viscous-type form with

$$\gamma_k = 0 \quad \text{at} \quad k \le k_c,$$

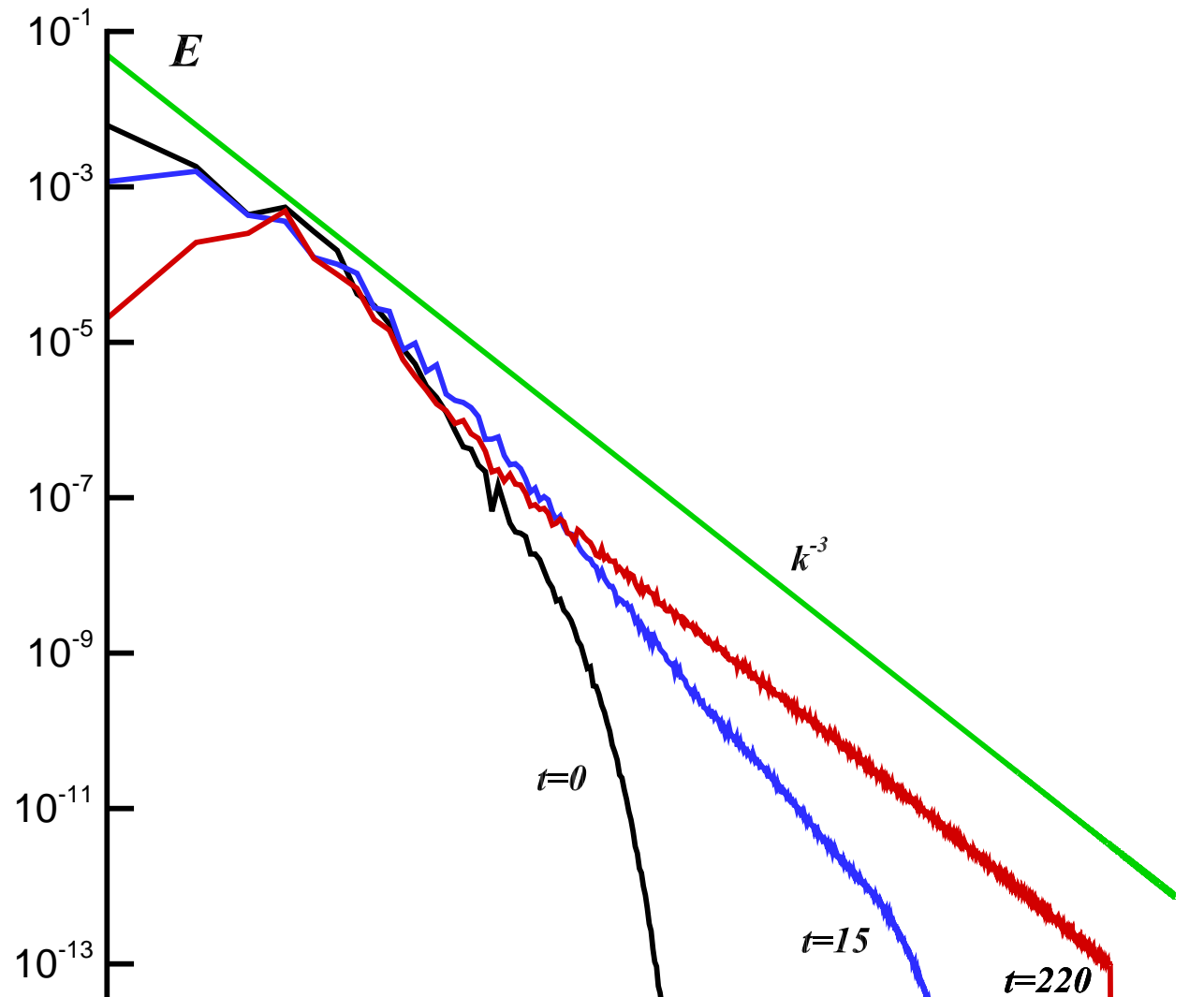$$\gamma_k = -\nu(k - k_c)^2 \quad \text{at} \quad k > k_c.$$

2D turbulence with pumping and damping
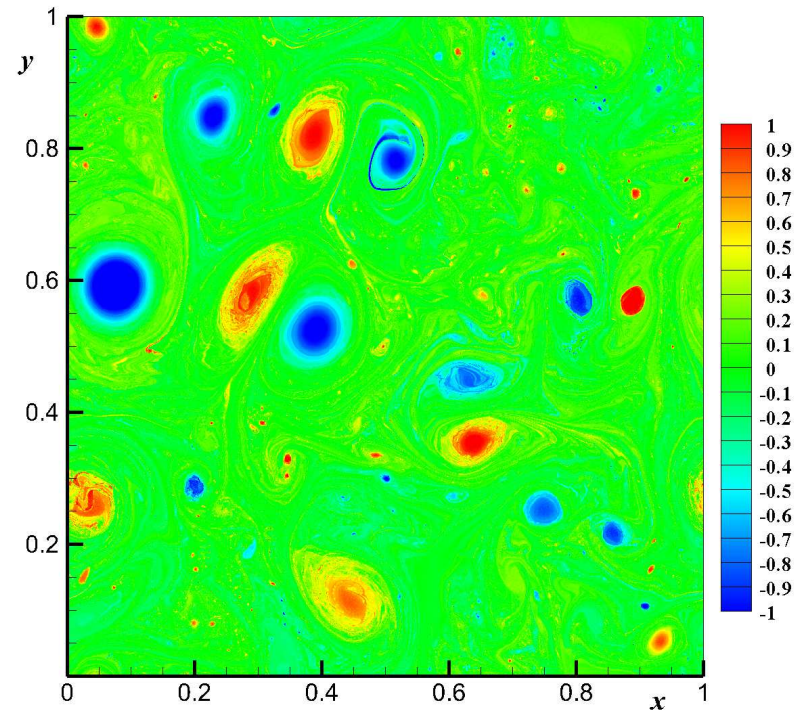
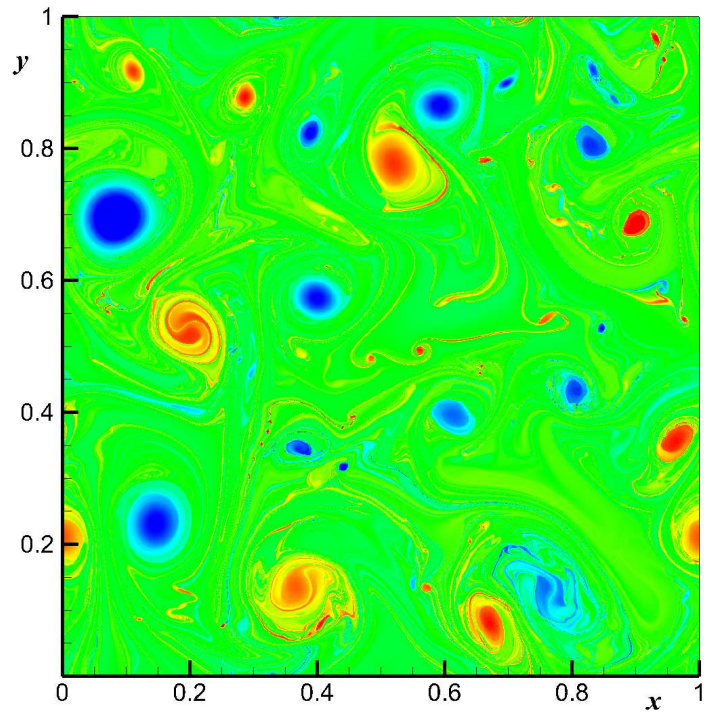Time evolution of total energy E and total enstrophy H
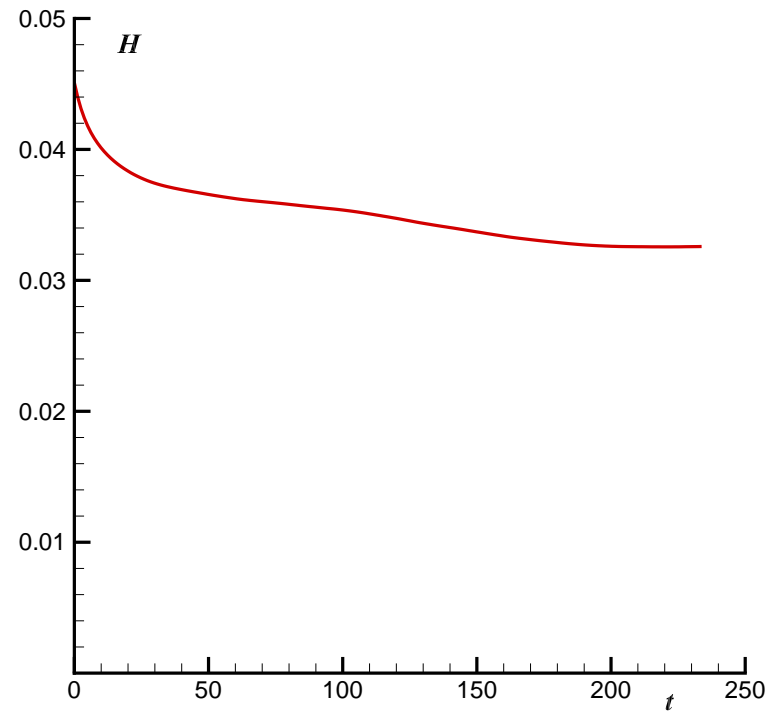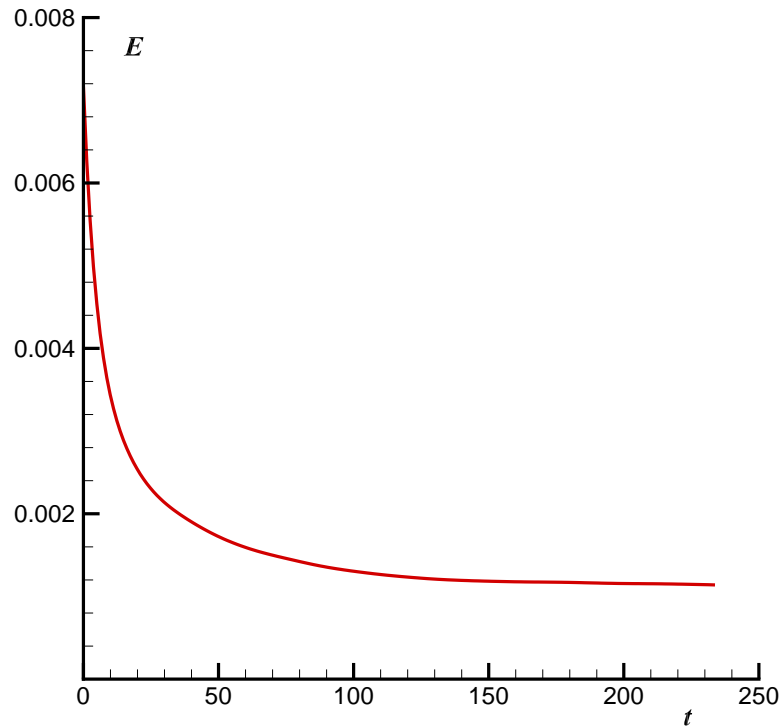
2D turbulence with pumping and damping

Energy spectrum $E(k)$ at different instants of time
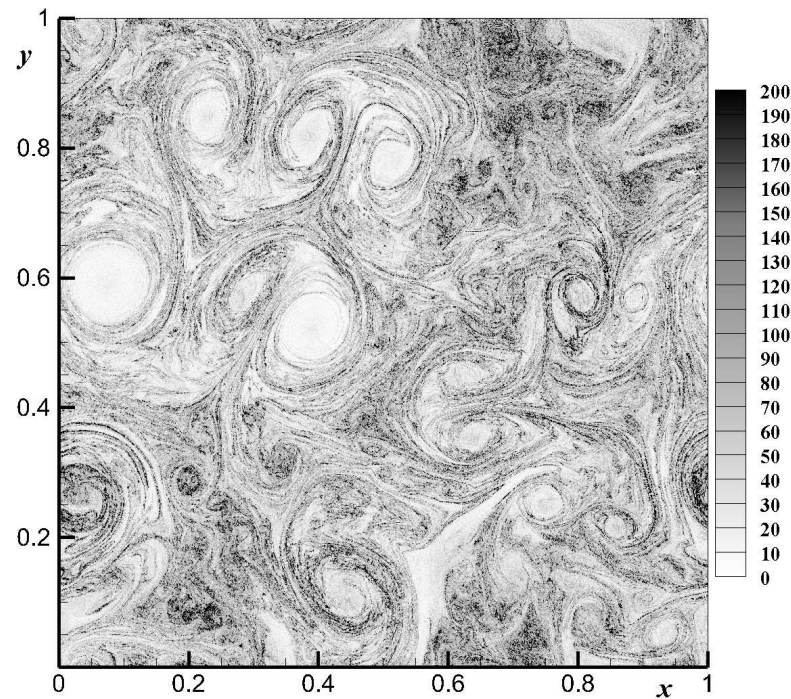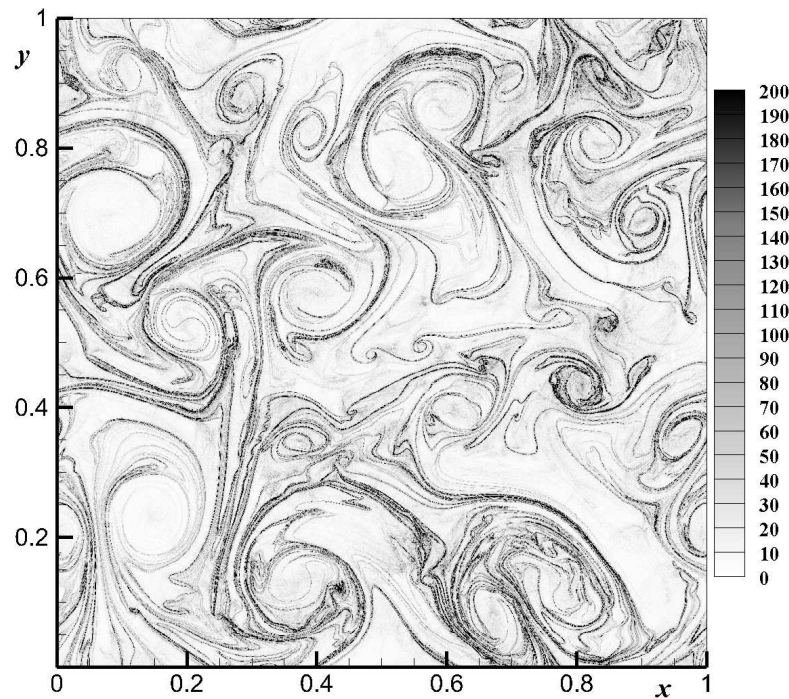
2D turbulence with pumping and damping

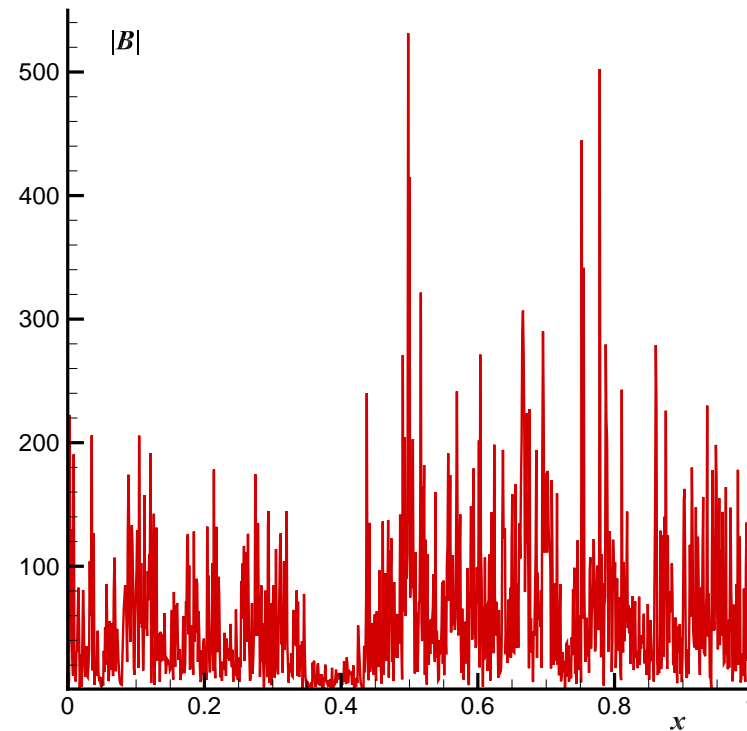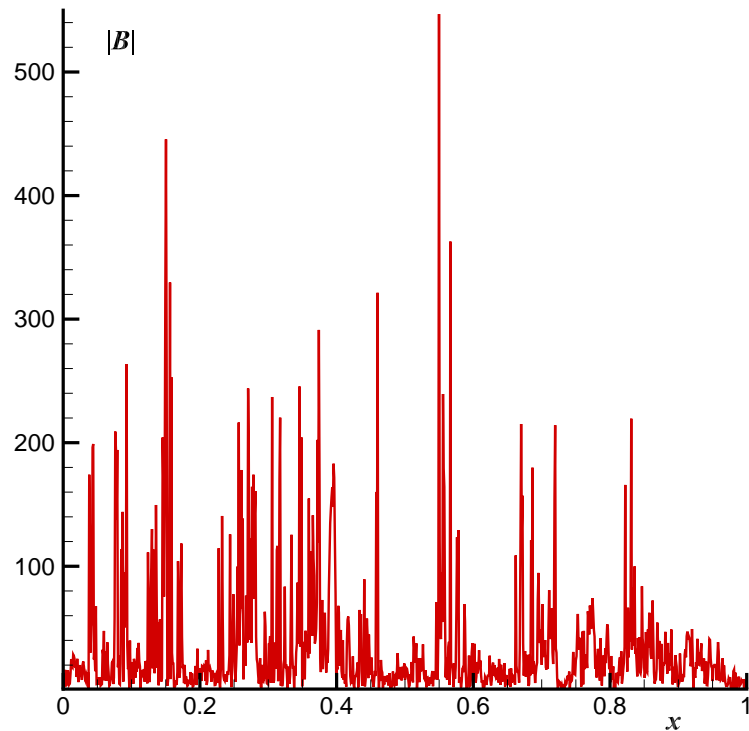Vorticity distributions at $t = 100, 220$

2D turbulence with pumping and damping

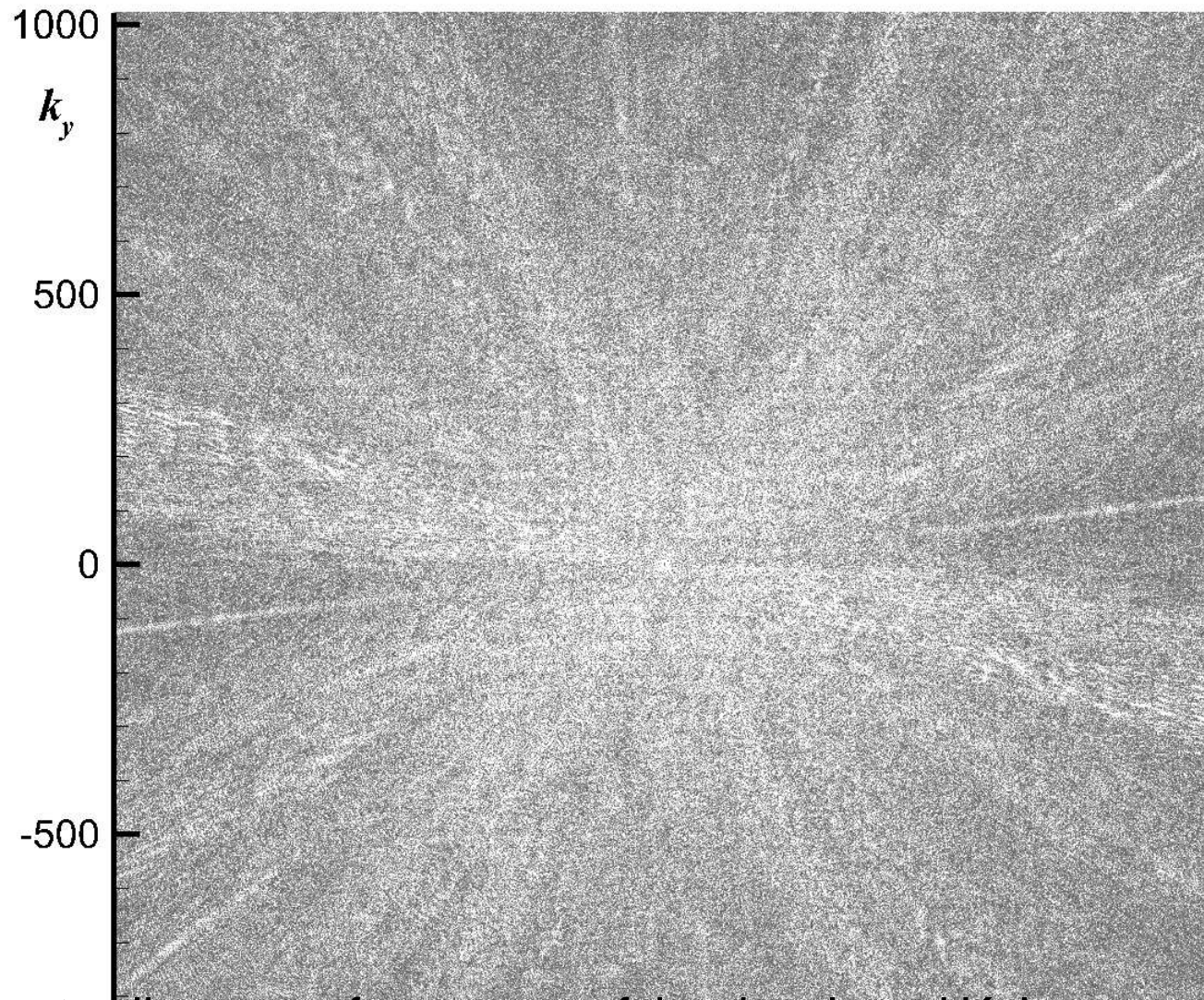## Distribution of $|\mathbf{B}|$ at $t = 100, 220$

2D turbulence with pumping and damping

Distribution of $|\mathbf{B}|$ along line $y = 0.5$ at $t = 100, 220$.
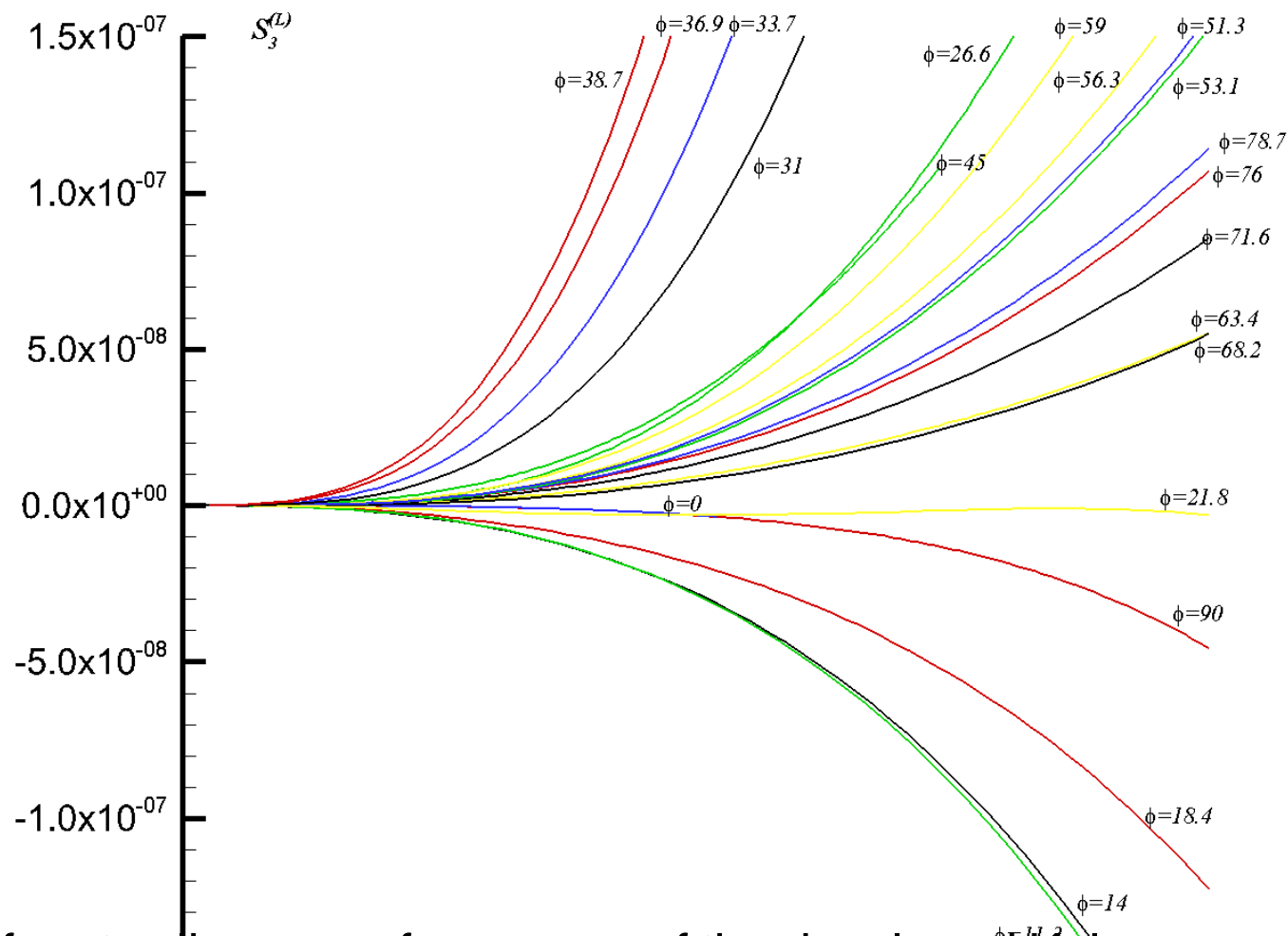
2D turbulence with pumping and damping

2D compensated spectrum $k^4 \epsilon(k_x, k_y)$ at $t = 220$

2D turbulence with pumping and damping

Dependence of $S_3^{(L)}$ as function of R at different angles.

2D turbulence with pumping and damping

At each angle $S_3^{(L)}(\mathbf{R})$ is close to the cubic parabola, i.e. $\propto R^3$, with a linear dependence relative η: $S_3^{(L)}(\mathbf{R}) \approx C_3 \eta R^3$. However, the average over angles of the third-order velocity structure function gives a significant difference with the constant $C_{3,isotr} = 1/8$ for the isotropic turbulence. It should be noted that the angular averaging constant C_3 undergoes temporal fluctuations: its maximal value sometimes reaches 5 (for this «steady» state!). Average over time within window $210 \geq t \leq 465$ with characteristic period $\simeq 17$ gives better correspondence: $\bar{C}_3 \simeq 2.4 C_{3,isotr}$.

Conclusion of the 2nd part

- Numerical simulations of the 2D freely-decaying isotropic turbulence have been performed using a pseudospectral Fourier method with the resolution up to 8192×8192.

- Formation of sharp vorticity gradients, which we call the vorticity quasi-shocks, has been observed.

- A Kraichnan-type direct enstrophy cascade with the fall-off k^{-3}-spectrum has been found.

- By means of the spatial filtering we have verified that this spectrum is appeared due to the formation of the vorticity quasi-shocks.

Conclusion of the 2nd part

- The strong angular dependence of the spectrum appearing due to a set of jets with a weak and/or strong overlapping has been observed.

- The structure function of third order shows a good correspondence to the Kraichnan direct cascade picture with the constant enstrophy flux. Powers ζ_n for higher structure functions grow weaker the linear dependence relative to n, demonstrating the intermittency

References

1. E.A. Kuznetsov, V.P. Ruban, *Hamiltonian dynamics of vortex lines for systems of the hydrodynamic type*, JETP Letters, **67**, 1076-1081 (1998); *Hamiltonian dynamics of vortex and magnetic lines in the hydrodynamic type models*, Phys. Rev E, **61**, 831-841 (2000).

2. E.A. Kuznetsov, *Vortex line representation for flows of ideal and viscous fluids* , JETP Letters, **76**, 346-350 (2002); physics/0209047.

3. D.S. Agafontsev, E.A. Kuznetsov and A.A. Mailybaev), *Development of high vorticity structures in incompressible 3D Euler equations*, Physics of Fluids **27**, 085102 (2015).

4. A.N. Kudryavtsev, E.A. Kuznetsov, and E.V. Sereshchenko, *Statistical features of freely decaying*

References

6. E.A. Kuznetsov, T. Passot and P.L. Sulem, *Compressible dynamics of magnetic field lines for incompressible MHD flows*, Physics of Plasmas, **11**, 1410-1415 (2004); physics/0310006.

7. E.A. Kuznetsov, V. Naulin, A.H. Nielsen, and J.J. Rasmussen, *Effects of sharp vorticity gradients in two-dimensional hydrodynamic turbulence*, Phys Fluids **19**, 105110 (2007) (10 pages).

8. E.A. Kuznetsov, V. Naulin, A.H. Nielsen, and J.J. Rasmussen, *Sharp vorticity gradients in two-dimensional turbulence and the energy spectrum*, Theor. Comput. Fluid Dyn., 24(1-4), 253-258 (2010) doi:10.1007/s00162-009-0135-4.

THANKS